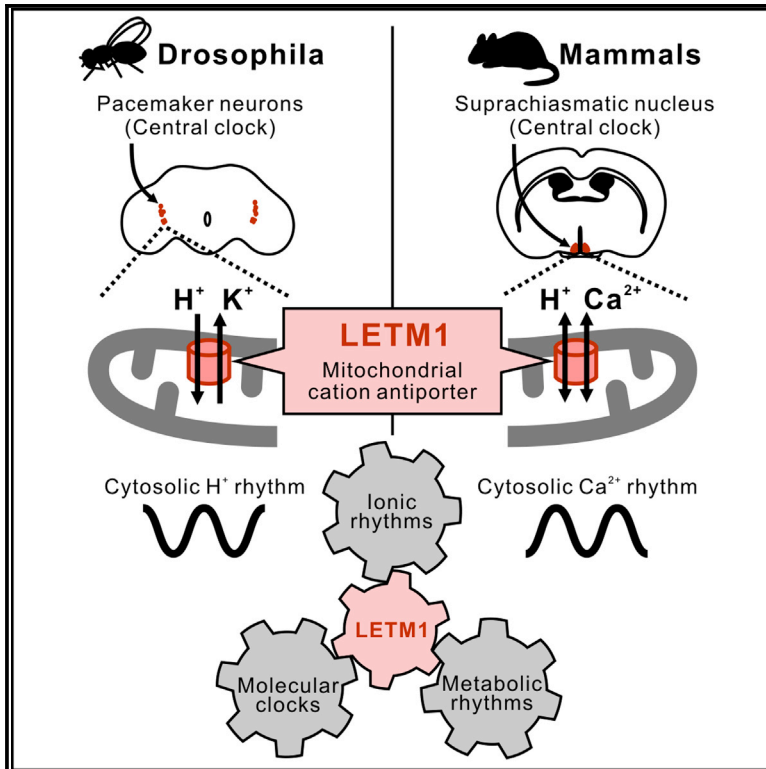


Mitochondrial LETM1 drives ionic and molecular clock rhythms in circadian pacemaker neurons

Graphical abstract



Authors

Eri Morioka, Yusuke Kasuga, Yuzuki Kanda, ..., Haruhiro Higashida, Todd C. Holmes, Masayuki Ikeda

Correspondence

msikeda@sci.u-toyama.ac.jp

In brief

Morioka et al. show critical functions of the mitochondrial cation antiporter LETM1 in cytosolic H⁺ and Ca²⁺ rhythms in *Drosophila* and rat circadian pacemaker neurons. LETM1 knockdown disturbs clock gene oscillations in both species, clarifying the mitochondrial coordination of clock function in pacemaker neurons.

Highlights

- Circadian cytosolic H⁺ rhythms are present in lateral neurons in *Drosophila*
- Circadian Ca²⁺ rhythms are present in rat suprachiasmatic nucleus neurons
- The mitochondrial cation antiporter LETM1 drives these ionic rhythms
- Clock gene oscillations in these circadian pacemakers also depend on LETM1

Article

Mitochondrial LETM1 drives ionic and molecular clock rhythms in circadian pacemaker neurons

Eri Morioka,¹ Yusuke Kasuga,¹ Yuzuki Kanda,¹ Saki Moritama,¹ Hayato Koizumi,² Tomoko Yoshikawa,³ Nobuhiko Miura,⁴ Masaaki Ikeda,⁵ Haruhiro Higashida,⁶ Todd C. Holmes,⁷ and Masayuki Ikeda^{2,3,8,*}

¹Graduate School of Science and Engineering, University of Toyama, Gofuku, Toyama 930-8555, Japan

²Graduate School of Innovative Life Science, University of Toyama, Gofuku, Toyama 930-8555, Japan

³Organization for International Education and Exchange, University of Toyama, Toyama 930-8555, Japan

⁴Department of Health Medicine, Yokohama University of Pharmacy, Yokohama, Kanagawa 245-0061, Japan

⁵Department of Physiology, Faculty of Medicine, Saitama Medical University, Saitama 350-0495, Japan

⁶Research Center for Child Mental Development, Kanazawa University, Ishikawa 920-8640, Japan

⁷Department of Physiology and Biophysics, School of Medicine, University of California, Irvine, CA 92697, USA

⁸Lead contact

*Correspondence: msikeda@sci.u-toyama.ac.jp

<https://doi.org/10.1016/j.celrep.2022.110787>

SUMMARY

The mechanisms that generate robust ionic oscillation in circadian pacemaker neurons are under investigation. Here, we demonstrate critical functions of the mitochondrial cation antiporter leucine zipper-EF-hand-containing transmembrane protein 1 (LETM1), which exchanges K^+/H^+ in *Drosophila* and Ca^{2+}/H^+ in mammals, in circadian pacemaker neurons. *Letm1* knockdown in *Drosophila* pacemaker neurons reduced circadian cytosolic H^+ rhythms and prolonged nuclear PERIOD/TIMELESS expression rhythms and locomotor activity rhythms. In rat pacemaker neurons in the hypothalamic suprachiasmatic nucleus (SCN), circadian rhythms in cytosolic Ca^{2+} and *Bmal1* transcription were dampened by *Letm1* knockdown. Mitochondrial Ca^{2+} uptake peaks late during the day were also observed in rat SCN neurons following photolytic elevation of cytosolic Ca^{2+} . Since cation transport by LETM1 is coupled to mitochondrial energy synthesis, we propose that LETM1 integrates metabolic, ionic, and molecular clock rhythms in the central clock system in both

Q2 invertebrates and vertebrates.

Q3 Q4 Q7 INTRODUCTION Q8

Various cellular activities are regulated by circadian clocks that optimize activities and help anticipate and respond to cyclic environmental changes (Partch et al., 2014). Cellular metabolic activity displays circadian rhythms, and rhythmicity in ATP synthesis has been demonstrated in numerous cell types, from fibroblasts to plants cells (Schmitt et al., 2018; Reinke and Asher, 2019). The core oscillatory mechanisms have been described by transcriptional-translational feedback loops (TTFLs) among clock genes [such as *Period* (*Per*)1/2, *Bmal1*, *Clock*, and *Cryptochrome* (*Cry*) in mammals] (Dunlap, 1999; Reppert and Weaver, 2002). Indeed, deletion of clock gene(s) flattens most cellular circadian oscillations, including metabolic rhythms (Marcheva et al., 2013). Circadian metabolic activities feed back to influence TTFLs, as they are sensitive to metabolic signals such as nicotinamide adenine dinucleotide (NAD) status. The $NAD^+/NADH$ ratio influences binding of the E-box in the CLOCK-BMAL1 heterodimer with NAD-dependent enzymes such as sirtuin-1 and poly ADP-ribose polymerase-1 (Rutter et al., 2001; Nakahata et al., 2008; Ramsey et al., 2009). Additionally, AMP-dependent protein kinase senses the ATP/AMP ratio and directly phosphorylates CRY, which eventually influences protein degradation of

PERIOD (PER) in TTFLs (Lamia et al., 2009). Thus, it seems likely that molecular clock movements are closely associated with cellular metabolic cycles.

Although nuclear-independent redox circadian oscillations have been observed in various cells, from human red blood cells to bacteria (O'Neill and Reddy, 2011; Edgar et al., 2012; Hoyle and O'Neill, 2015), bioenergetic activities in mitochondria could be a strong feedback signal to TTFLs in eukaryotic cells. Indeed, a recent study by Schmitt et al. (2018) demonstrated the critical role of dynamin-related protein 1 (DRP1) in circadian regulation. DRP1 is essential not only for the generation of circadian rhythms in mitochondrial fusion/fission and ATP synthesis but also for the oscillation of TTFLs in fibroblasts (Schmitt et al., 2018). The mitochondrion is not only the location of ATP synthesis but also an organelle that buffers and transports intracellular ions. It is widely accepted that mitochondrial H^+ transport across the inner membrane occurs during ATP synthesis, whereas other cations such as Na^+ , K^+ , and Ca^{2+} are also actively transported through the mitochondrial inner membrane (Bernardi, 1999). However, the link between metabolic rhythms, TTFLs, and mitochondrial ion flux remains unclear.

Although clock gene TTFLs are found in numerous cell types in animals (Balsalobre et al., 1998; Zylka et al., 1998; Yamazaki

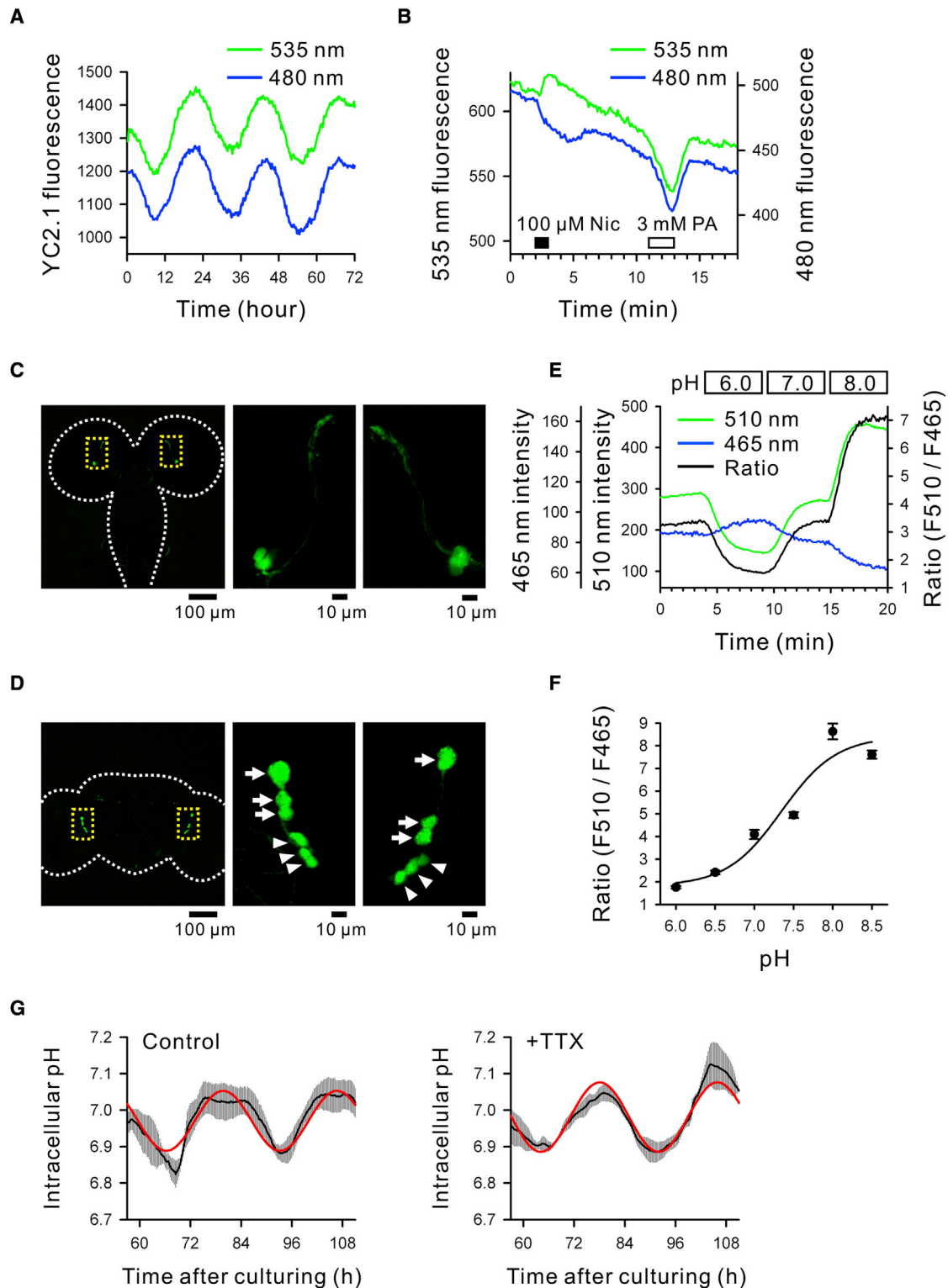


Figure 1. Circadian rhythms in cytosolic H^+ concentrations in *Drosophila* circadian pacemaker neurons

(A) Ratiometric Ca^{2+} analysis was performed by TIMELESS-driven YC2.1 expression in pupal LNs in *cry^b* background flies. However, YC2.1 displayed unique circadian rhythms in fluorescence with donor (480 nm, blue trace) and acceptor (535 nm, green trace) oscillating in a tandem fashion.

(legend continued on next page)

et al., 2000), central circadian pacemaker neurons are particularly critical for the integration of peripheral oscillators and the manifestation of overt behavioral rhythms (Mohawk et al., 2012). Mammalian circadian pacemaker neurons are located within the hypothalamic suprachiasmatic nucleus (SCN) (Stephan and Zucker, 1972; Moore and Eichler, 1972) and exhibit spontaneous circadian oscillations in action potential firing frequencies even in *in vitro* setups (Green and Gillette, 1982; Welsh et al., 1995). Central pacemaker neurons display more stable TTFLs than peripheral cells (Yamazaki et al., 2000; Abe et al., 2002; Versteven et al., 2020), although the differences between central pacemakers and peripheral oscillators remain obscure. The stability of TTFLs in the mammalian circadian pacemaker can be explained by tight neural networks in SCN neurons (Liu et al., 2007; Leise et al., 2012; Noguchi et al., 2017), whereas network structures are widely variable among animal species. Our group has demonstrated the presence of robust circadian rhythms in cytosolic Ca^{2+} concentrations in mouse SCN neurons (Ikeda et al., 2003). This circadian Ca^{2+} rhythm is maintained even after the blockade of action potentials by tetrodotoxin (TTX) and is observed exclusively in the SCN (Ikeda et al., 2003; Enoki et al., 2012). However, the mechanisms that generate this ultra-low-frequency Ca^{2+} oscillation are unknown.

The presence of robust circadian rhythms in cytosolic Ca^{2+} concentration is hypothesized as a common feature of oscillating cells across a wide variety of organisms (Harrisingh and Nitabach, 2008), including *Drosophila* pacemaker neurons (lateral neurons; LNs) (Liang et al., 2016). We investigated circadian cytosolic Ca^{2+} rhythms in LNs *in vitro*; however, we observed dynamic circadian rhythms in H^{+} concentration, rather than Ca^{2+} concentration, using the classical Yellow Cameleon Ca^{2+} sensor (YC2.1; Figures 1A and 1B). By screening *Drosophila* mutants and analyzing rat SCN neurons, we conclude here that the leucine zipper-EF-hand-containing transmembrane protein 1 (LETM1), a mitochondrial cation antiporter that exchanges $\text{K}^{+}/\text{H}^{+}$ in *Drosophila* (McQuibban et al., 2010) and $\text{Ca}^{2+}/\text{H}^{+}$ in mammals (Jiang et al., 2013), plays an essential role in the generation of circadian ionic rhythms in pacemaker neurons. Moreover, because knockdown of *Letm1* influences clock gene TTFLs in LNs and SCN neurons, we propose a critical role for LETM1 in the integration of metabolic, ionic, and molecular clock rhythms in the central clock system.

RESULTS

LETM1-dependent circadian rhythms in cytosolic H^{+} concentration in *Drosophila* pacemaker neurons

In our examination of circadian cytosolic Ca^{2+} rhythms in pupal LN cultures, we unexpectedly observed unique changes in YC2.1 fluorescence, where fluorescence intensities of 480 nm (donor) and 535 nm (acceptor) oscillated in tandem in a circadian fashion (Figure 1A). This does not imply that the YC2.1 sensor expressed in LNs was not functioning properly in *Drosophila*, because fluorescence resonance energy transfer (FRET), with a reduction in donor fluorescence and an increase in acceptor fluorescence, occurred as expected when LNs were stimulated with nicotine (Figure 1B). Additionally, we previously used the same sensor in *Drosophila* endocrine cells to detect Ca^{2+} -spiking activities, with no problems with FRET (Morioka et al., 2012). The parallel changes in donor and acceptor were observed when cells were exposed to an acidic environment (Figure 1B), in agreement with the basic characteristics of green fluorescent protein (GFP) mutants (Wachter et al., 1997; Patterson et al., 1997; Miyawaki et al., 1999). To investigate the circadian rhythms in pH in LNs, we generated a fly line expressing the ratiometric proton sensor deGFP4 (Hanson et al., 2002) (Figures 1C–1F), which confirmed circadian pH rhythms in LN culture (Figure 1G). The circadian pH rhythms were not sensitive to TTX (Figure 1G), which suggests intrinsic oscillation within the LNs.

Because action potential firing of large ventral lateral neurons (LN_vs) in adult flies is sensitive to pH perturbations (Figures 2A and 2B), circadian pH rhythms in LNs, if any in adults, can theoretically influence circadian behavioral rhythms. With locomotor activity monitoring of various mutant flies under constant darkness (DD), we found significant prolongation of the free-running period in flies carrying RNAi for *Letm1* ($\tau = 25.65 \pm 0.07$ h in *Pdf-Gal4;UAS-Dicer2;UAS-Letm1^{RNAi}*, 2-h extension of the period compared with the control, $F_{12,374} = 72.50$, $p < 0.001$ by one-way ANOVA; Figures 3A, 3B, and S1A and Table S1). RNAi reduced *Letm1* mRNA expression by 60% compared with that in control flies (Figure 3C). For quantitative estimation of LETM1 function, we compared the size of the cytosolic H^{+} influx following treatment with a protonophore (CCCP) in pupal LN cultures kept under 12:12-h light-dark (LD) cycles (Figure 3D). A peak in CCCP-induced H^{+} influx was observed late during the daytime (zeitgeber time 8; ZT8), whereas a

(B) The effects of nicotine (Nic, 100 μM) and propionic acid (PA, 3 mM) were analyzed using the sample in (A). Proper FRET (opposing intensity changes between donor and acceptor) was induced upon Nic stimulation, whereas intentional acidification by PA caused a parallel decrease in fluorescence. Data are representative of 5–10 independent experiments.

(C) Representative images of *Pdf*-driven deGFP4 expressions in the pupal CNS (white dotted line). The fluorescent signal was concentrated in pacemaker neurons (LNs). Enlarged images within the boxed areas (yellow dotted lines) are shown on the right.

(D) Representative images of *Pdf*-driven deGFP4 expression in the adult fly brain (white dotted line), also showing fluorescent signals concentrated in pacemaker neurons. Enlarged images within the boxed areas (yellow dotted lines) on the right identify large LN_vs (arrows) and small LN_vs (arrowheads).

(E) Ratiometric deGFP4 fluorescence (F510/F465 nm) intensities in pupal LN cultures for pH calibration. Three step changes in extracellular pH levels were applied with high $[\text{K}^{+}]$ and 1 μM nigericin-containing solution. Theoretical opposing intensity changes were successfully induced.

(F) The pH-dependent curve fitted for the deGFP4 fluorescence ratio. $n = 5$ –17 for each data point.

(G) Long-term time-lapse imaging of deGFP4 in pupal LN cultures. Data are presented as the mean \pm SEM of three independent experiments. The circadian acidification rhythms were observed in standard culture medium (left) and in culture medium supplemented with TTX (300 nM, right). To reduce the impact of excitation light (405 nm), these experiments were performed using *Pdf*-driven deGFP4 in *cry²* background flies. Statistical sine curve fittings were performed (red lines). $\tau = 26.92$ h ($p < 0.01$) for the control and 27.85 h ($p < 0.01$) for the TTX group.

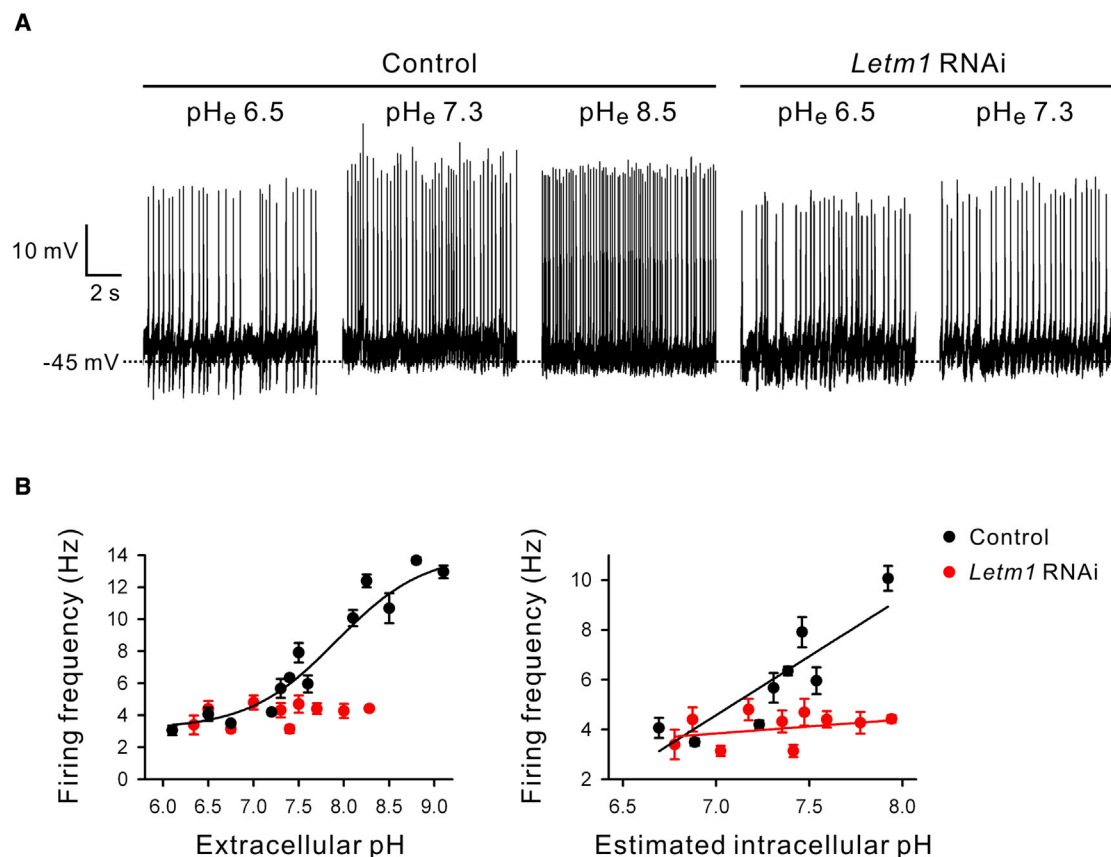


Figure 2. pH dependence of spontaneous firing rates in *Drosophila* circadian pacemaker neurons

(A) Representative whole-cell current clamp recordings for 10 s in large LN_vs of adult flies in different extracellular pH conditions in control and *Letm1* knockdown flies (*pdfGal4-p12c;UAS-Letm1^{RNAi}*).

(B) The extracellular pH-dependent curve for action potential firing frequencies in large LN_vs was fitted by the four-parameter Hill function. The intracellular pH (right) was estimated on the basis of the deGFP4 fluorescence intensity, and a linear regression curve was fitted on the basis of its dependence. n = 9–39 control flies and n = 18–54 *Letm1* knockdown flies.

trough was observed late during the nighttime (ZT20) (Figure 3E). Calibration of pH in a separate set of experiments determined the dynamic range of this H⁺ flux and revealed cyclic acidification during the nighttime in pupal LN_vs (Figures 3D and 3E). Notably, the pH rhythm in LN_vs was significantly flattened by *Letm1* RNAi (in *Pdf-Gal4;UAS-deGFP4;UAS-Letm1^{RNAi}* compared with the control [*Pdf-Gal4;UAS-deGFP4*], $F_{7,582} = 5.37$, $p < 0.001$ by two-way ANOVA, interaction between time and genotype; Figure 3E). Among the RNAi strains examined, daytime acidification was exclusively observed in the *Letm1* RNAi strain (Figure S1B). Consistently, the action potential firing frequencies of large LN_vs in adult *Letm1* knockdown flies (4.32 ± 0.45 Hz in *pdfGal4-p12c;UAS-Letm1^{RNAi}*) were significantly lower than those in control flies (5.67 ± 0.60 Hz in *pdfGal4-p12c*, $p < 0.05$ by Student's t test) in the middle of the day at pHe 7.3 (Figures 2A and 2B). Taken together, these results demonstrate that LETM1 drives action potential firing rhythms and behavioral rhythms in *Drosophila* as an essential mediator of the circadian pH rhythms in LN_vs.

LETM1-dependent circadian rhythms in nuclear PER/TIM expression in *Drosophila* pacemaker neurons

Next, we analyzed canonical clock gene oscillations in adult LN_vs in *Letm1* knockdown flies by immunofluorescent staining of nuclear PER and TIMELESS (TIM) (Figure 4). Small LN_vs exhibited oscillations of relatively larger amplitude in nuclear PER and TIM expression, and *Letm1* knockdown had a limited effect on their magnitude (Figure 4A). The peak PER/TIM expression, however, was delayed by approximately 3–4 h on the fourth day under DD, consistent with prolongation of behavioral rhythms under DD. Nuclear PER in large LN_vs displayed smaller circadian variations and was difficult to fit with a sine curve using the CircWave algorithm ($p > 0.05$). Nevertheless, nuclear PER displayed an overall reduction in expression levels in *Letm1* knockdown flies ($F_{1,420} = 5.46$, $p < 0.05$, two-way ANOVA, between genotypes; Figure 4B). Nuclear TIM rhythms in large LN_vs displayed less circadian variation, and significant differences between the genotypes were not observed ($F_{1,480} = 0.23$, $p = 0.63$, two-way ANOVA; Figure 4B).

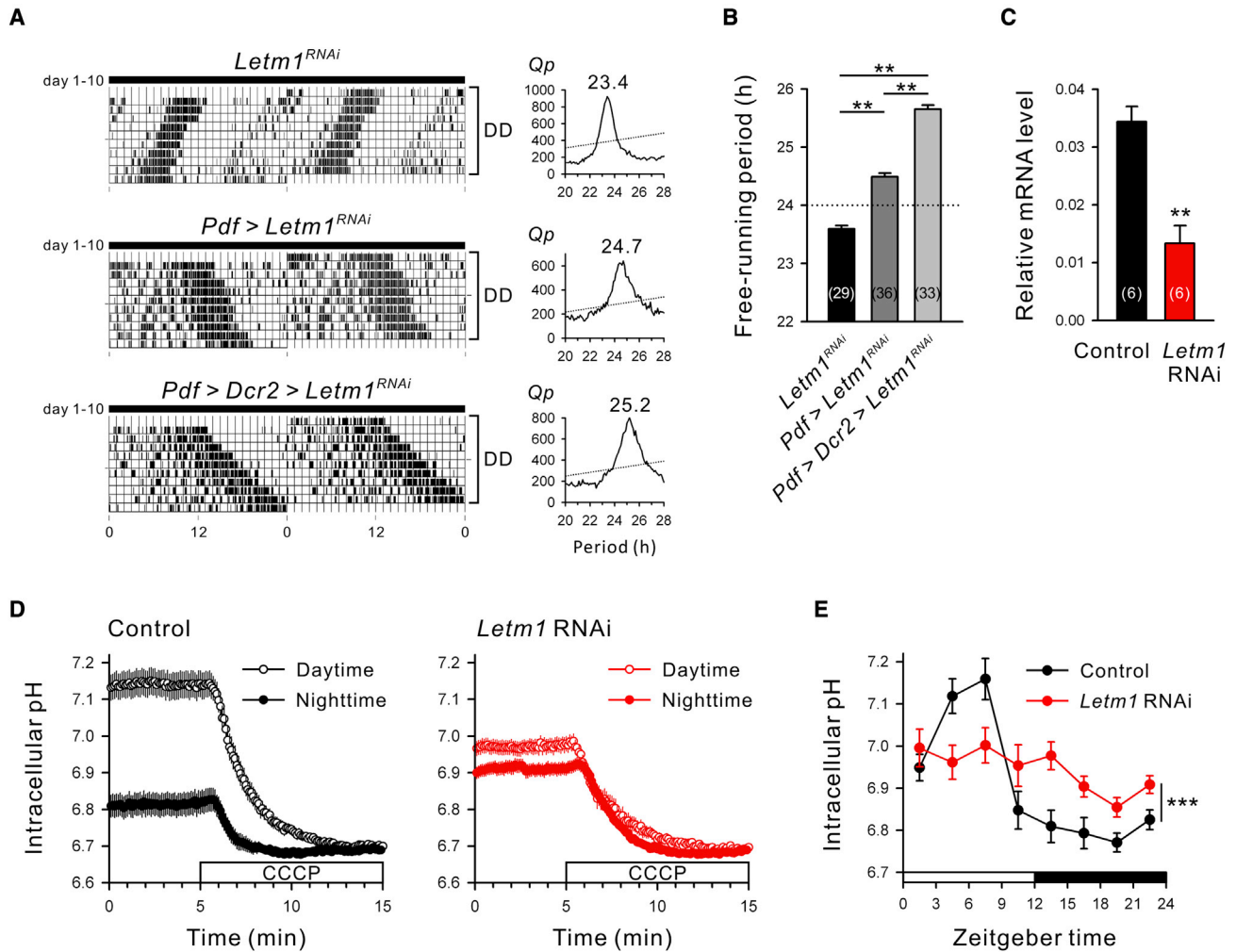


Figure 3. *Letm1* knockdown lengthens the free-running period of circadian locomotor rhythms and suppresses intracellular pH rhythms in *Drosophila* pacemaker neurons

(A) Representative actograms (left) and Chi-square periodograms (right) for flies with the following genotypes: control (*UAS-Letm1^{RNAi}*), *Pdf*-driven *Letm1* knockdown (*Pdf-Gal4;UAS-Letm1^{RNAi}*), and *Pdf*-driven *Letm1* knockdown with additional *UAS-Dicer2* transgene.

(B) Average free-running periods under DD in control and *Pdf*-driven *Letm1* knockdown flies. Number in parentheses denotes the number of flies used for experiments. ***p* < 0.01 by Bonferroni's test following one-way ANOVA.

(C) *Letm1* mRNA expression levels in fly brains from the control (*UAS-Letm1^{RNAi}*) and *Elav*-driven *Letm1* knockdown (*Elav-Gal4/CyO;UAS-Letm1^{RNAi}*) groups were evaluated using real-time RT-PCR assays. The relative expression levels of *rp49* were compared. ***p* < 0.01 by the Mann-Whitney U test.

(D) Effects of CCCP on intracellular pH (pH_i) in pupal LN cultures during the daytime (ZT5–7, open circle) and nighttime (ZT12–24, filled circle). These experiments were performed using control flies (*Pdf-Gal4;UAS-deGFP4*, left) and *pdf*-driven *Letm1* knockdown flies (*Pdf-Gal4;UAS-deGFP4;UAS-Letm1^{RNAi}*, right). Note that addition of 10 μM CCCP decreased pH_i to the steady value via H⁺ equilibration regardless of time or genotype, enabling the estimation of intrinsic variations in pH_i.

(E) Plots of the day-night variations in pH_i in LNs of control flies (black) and *pdf*-driven *Letm1* RNAi (red) flies. The circadian acidification rhythms were estimated in control flies, whereas the rhythm was lacking in *Letm1* RNAi flies. Two-way ANOVA revealed a significant difference (***p* < 0.001) between control and *Letm1* RNAi flies. The white and black bars on the bottom indicate the light and dark periods, respectively. Data are presented as mean ± SEM. *n* = 29–47 per time point.

LETM1-dependent rhythms in rat circadian pacemaker neurons and human model cells

The role of LETM1 in ionic and clock gene transcriptional rhythms was further studied using rat SCN neurons. Short hairpin RNA (shRNA) encoding *Letm1* in plasmid carrying red fluorescent protein (RFP) or control plasmid was co-transfected with plasmid carrying the YC3.6 Ca²⁺ sensor and/or a *Bmal1-luciferase* (*Bmal1-luc*) reporter using a gene gun in organotypic SCN cultures (Figure 5A). Co-transfection with *Letm1* shRNA

gradually dampened circadian cytosolic Ca²⁺ rhythms in SCN neurons during the first week after transfection (Figure 5B). On the seventh day, the amplitude of the circadian Ca²⁺ rhythm diminished to 40% of that in the control (*p* < 0.01, Student's *t* test). Additionally, the average circadian period of the Ca²⁺ rhythms prolonged to 24.9 ± 0.3 h 4–7 days after *Letm1* shRNA transfection, which was longer than the period in the control group (23.4 ± 0.2 h, *p* < 0.01, Student's *t* test). Additionally, chemiluminescence imaging demonstrated a significant

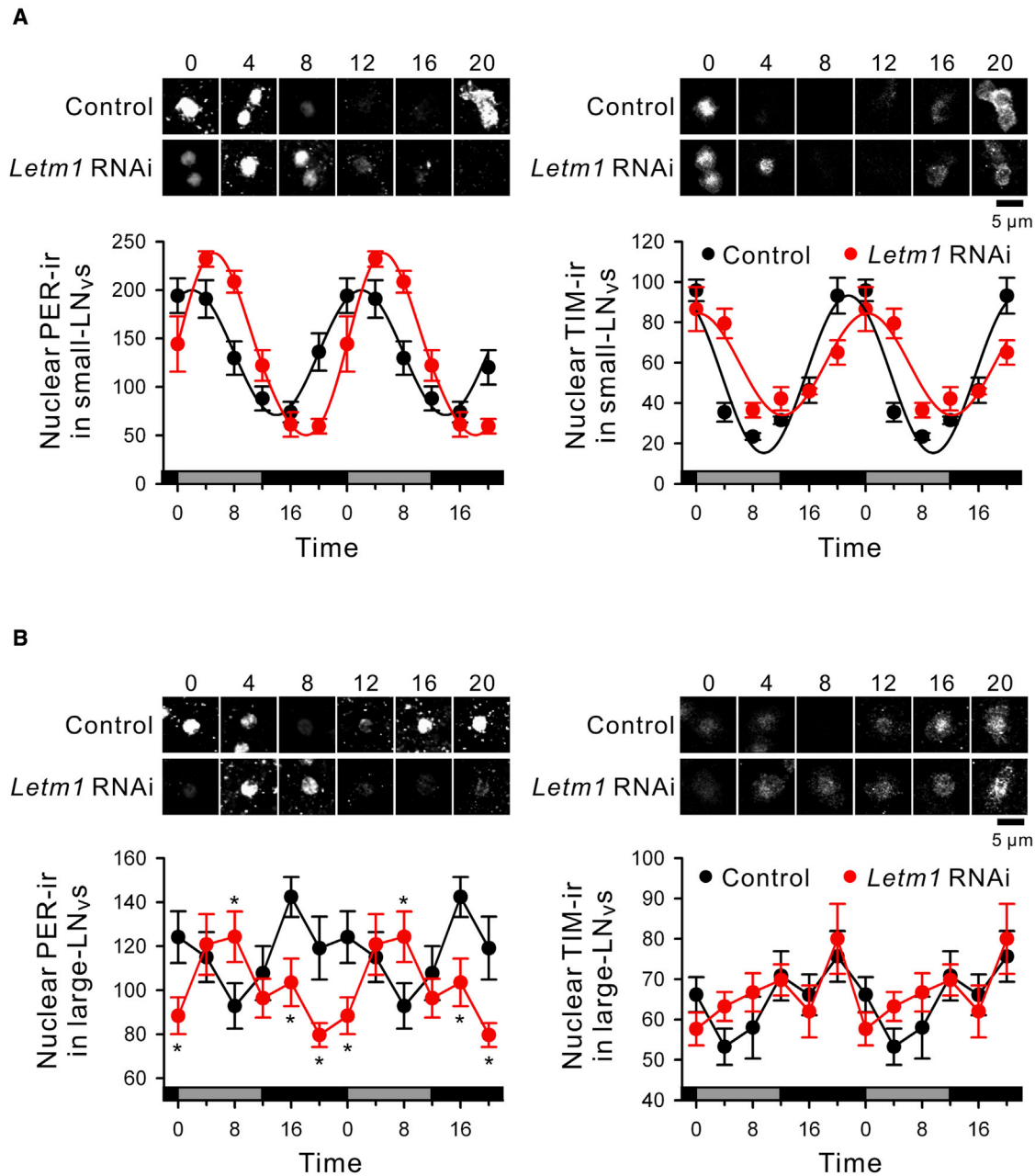


Figure 4. Nuclear PER and TIM expression patterns are altered by *Letm1* knockdown in *Drosophila* pacemaker neurons

(A) Top: Representative images of PER (left) and TIM (right) immunostaining in small LN_vs of adult flies. Images were acquired using flies on the fourth day under DD. Bottom: Nuclear-staining intensities were quantified and double plotted. Significant delays in nuclear PER and TIM expression rhythms were observed in *Letm1* knockdown flies. Data are presented as mean \pm SEM. $n = 13$ – 15 per time point. Sine curves were successfully fitted for anti-PER immunoreactivity (PER-ir) ($p < 0.01$) and TIM-ir ($p < 0.05$) in small-LN_vs.

(B) Similar analysis of (A) in large LN_vs, demonstrating a significant effect of *Letm1* knockdown on nuclear PER levels. Note that three of six data points represent smaller values in *Letm1* knockdown flies. * $p < 0.05$ by Tukey's *post hoc* test following two-way ANOVA. Circadian variations in nuclear PER and TIM levels were small in large LN_vs, and statistical curve fittings were not applicable. $n = 36$ – 41 per time point.

(-79.4%) reduction in the amplitude of *Bmal1-luc* rhythms during the first week after *Letm1* shRNA transfection ($F_{2,216} = 81.39$, $p < 0.01$, Tukey's *post hoc* test following one-way ANOVA; Figures 5C and 5E). Furthermore, unstable *Bmal1-luc* rhythms were induced by long-term (~ 1 month) *Letm1*

knockdown (Figure 5D). The average period in *Bmal1-luc* rhythms was significantly longer at 22–31 days after transfection (27.7 ± 1.7 h) compared with control (23.9 ± 0.3 h) or immediately after shRNA transfection (24.0 ± 0.3 h; $F_{2,216} = 7.70$, $p < 0.01$, Tukey's *post hoc* test following one-way ANOVA; Figure 5E). A

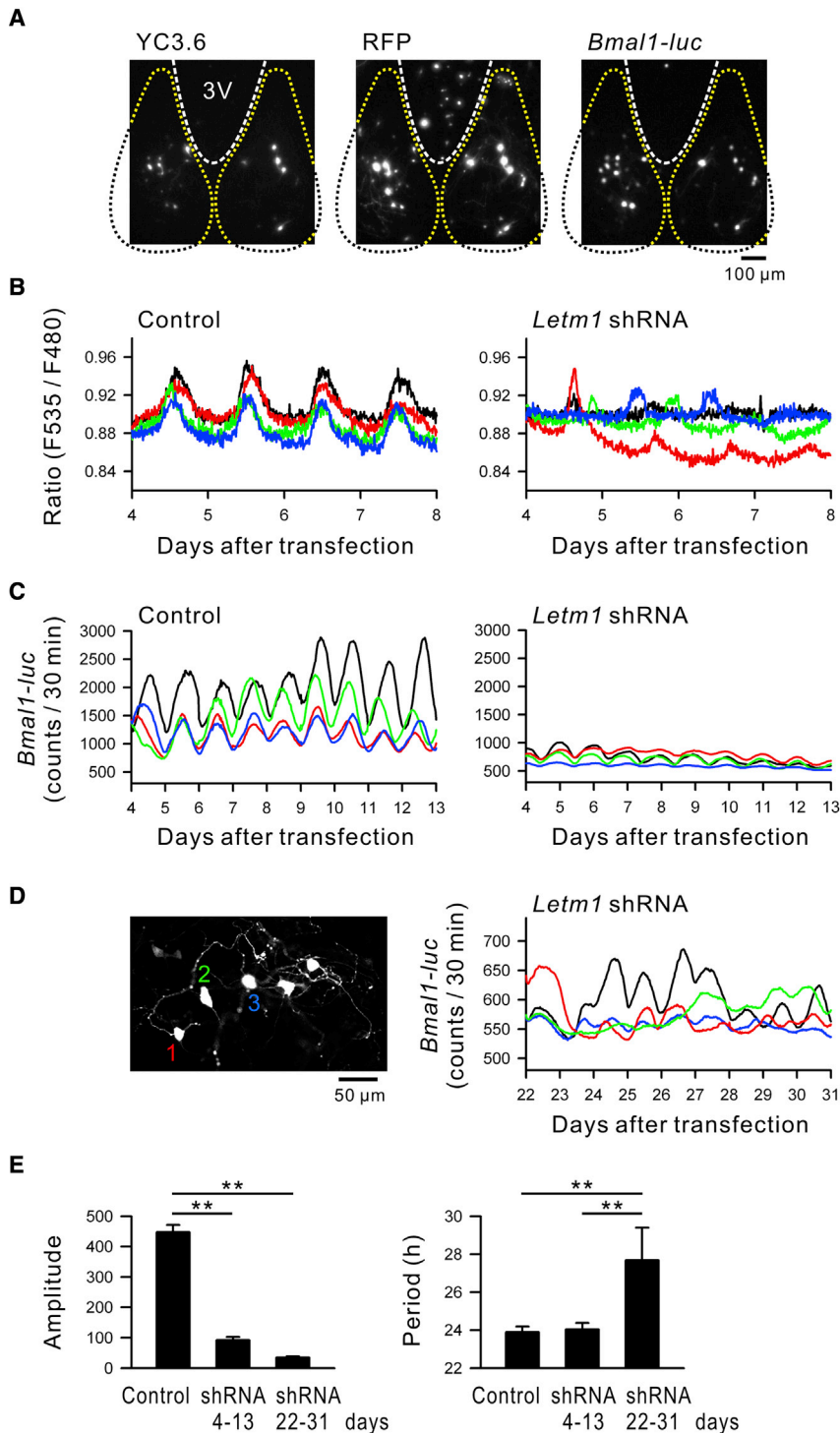


Figure 5. Effects of *Letm1* knockdown on circadian rhythms in cytosolic Ca^{2+} concentrations and *Bmal1* transcription in rat SCN neurons

(A) Ratiometric Ca^{2+} sensor (YC3.6) and *Bmal1-luc* were co-transfected with *Letm1* shRNA or its control vector using a gene gun in organotypic slice cultures of rat SCNs. Representative images demonstrating co-expression of *Letm1* shRNA (visualized by RFP) on YC3.6 and *Bmal1-luc* signals. Non-confocal images were acquired using a deep-cooled EM-CCD camera in a time-lapse imaging setup. Approximate borders of SCN regions are indicated by a yellow dotted line, and the third ventricle (3V) is indicated by a white dashed line. The greater RFP signals in the 3V are due to the promoter used (NSE promoter for YC3.6 and CMV promoter for RFP, *Letm1* shRNA). (B) Representative traces of cytosolic Ca^{2+} rhythms in four SCN neurons in the same organotypic culture. Note that co-transfection of *Letm1* shRNA caused progressive reduction in circadian cytosolic Ca^{2+} rhythms during the first week after transfection. Observations were reproducible for 19–28 neurons in three or four independent experiments.

(C) Representative traces of *Bmal1-luc* rhythms in four SCN neurons. Note that co-transfection of *Letm1* shRNA caused significant reductions in *Bmal1-luc* rhythms in SCN neurons.

(D) Unstable *Bmal1-luc* rhythms were produced by long-term (~ 1 month) *Letm1* knockdown. Intact neuronal morphologies (no dendritic swelling) were observed at the end of long-term chemiluminescence imaging. Fluorescence image (left) was acquired using RFP signals on a confocal-imaging setup. Red, green, and blue traces correspond to the signals from numbered neurons on the RFP image.

(E) Circadian amplitude (left) and period (right) of *Bmal1-luc* rhythms were statistically compared. The amplitude was immediately reduced after *Letm1* shRNA transfection, whereas the period was prolonged for a long time after shRNA transfection. $**p < 0.01$ by Tukey's *post hoc* test following one-way ANOVA. Observations were reproducible for 18–22 neurons in three or four independent experiments. Although the *Bmal1* promoter is occasionally activated in SCN glial cells, in the present analysis we counted signals only in neurons.

YC3.6 Ca^{2+} sensor (hRPE-YC) because it exhibits *Bmal1* transcriptional rhythms and circadian Ca^{2+} spiking rhythms after dexamethasone (Dex) treatment (Ikashi et al., 2017). Additionally, hRPE-YC cells stably expressing *Letm1* shRNA or its randomized shRNA were generated to compare phenotypes. We confirmed that

normal neuronal morphology, without dendritic swelling, was observed at the end of long-term *Letm1* knockdown experiments (Figures 5D and S2).

To analyze the mechanisms underlying ionic rhythm generation by LETM1, we used a human cell line, derived from retinal pigment epithelium, stably expressing *Bmal1-luc* and the

knockdown of *Letm1* decreased the expression of *Letm1* mRNA by 70% compared with control ($p < 0.05$, Mann-Whitney U test; Figure 6A). Consistently, immunofluorescence staining revealed that mitochondrial LETM1 protein decreased by 40% compared with that in the control group ($p < 0.01$, Student's t test; Figures 6B and 6C). Furthermore, knockdown of *Letm1*

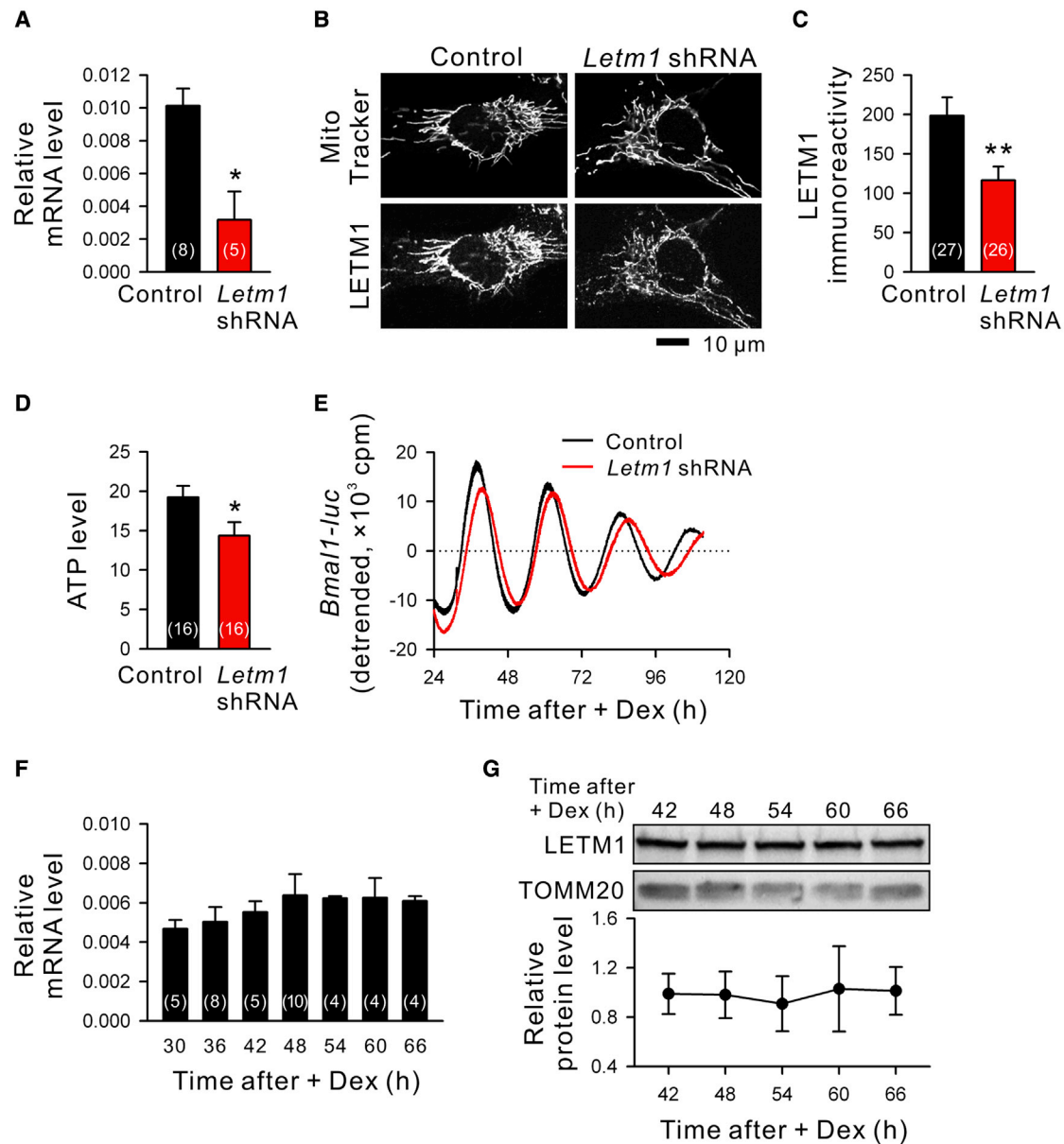


Figure 6. Effects of *Letm1* knockdown on transcriptional, translational, and ATP levels in human-model cells

(A) *Letm1* mRNA expression in hRPE-YC cells stably expressing scrambled shRNA or *Letm1* shRNA were evaluated using real-time RT-PCR. The relative expressions of β -actin were compared. * $p < 0.05$ by Mann-Whitney U test.

(B) Representative images of MitoTracker Red staining (top) and LETM1 immunostaining (bottom) in hRPE-YC cells stably expressing scrambled shRNA or *Letm1* shRNA.

(C) Mitochondrial LETM1 immunoreactivity levels were estimated as a function of mitochondrial dimension, which was visualized by MitoTracker Red. The averages were calculated from 26–27 images of four independent experiments. ** $p < 0.01$ by Student's t test.

(D) ATP content was compared between hRPE-YC cells stably expressing scrambled shRNA or *Letm1* shRNA. * $p < 0.05$ by Student's t test.

(E) *Bmal1-luc* rhythms were analyzed following Dex treatment. Note that *Bmal1* transcriptional rhythms were not significantly modulated by *Letm1* shRNA in hRPE-YC cells. Chemiluminescent signals from three dishes were normalized in this assay.

(F) Relative mRNA expression of *Letm1* was analyzed at different time points after Dex treatment. No circadian variations were found in *Letm1* expression in hRPE-YC cells. $p > 0.05$ by Kruskal-Wallis test.

(G) Mitochondrial LETM1 in hRPE-YC cells was analyzed by western blotting. Top: Representative blotting of LETM1 and control mitochondrial protein (TOMM20) is shown. Bottom: Quantification of LETM1 protein levels at different time points after Dex treatment demonstrated no circadian variations. $n = 4$, $p > 0.05$ by one-way ANOVA.

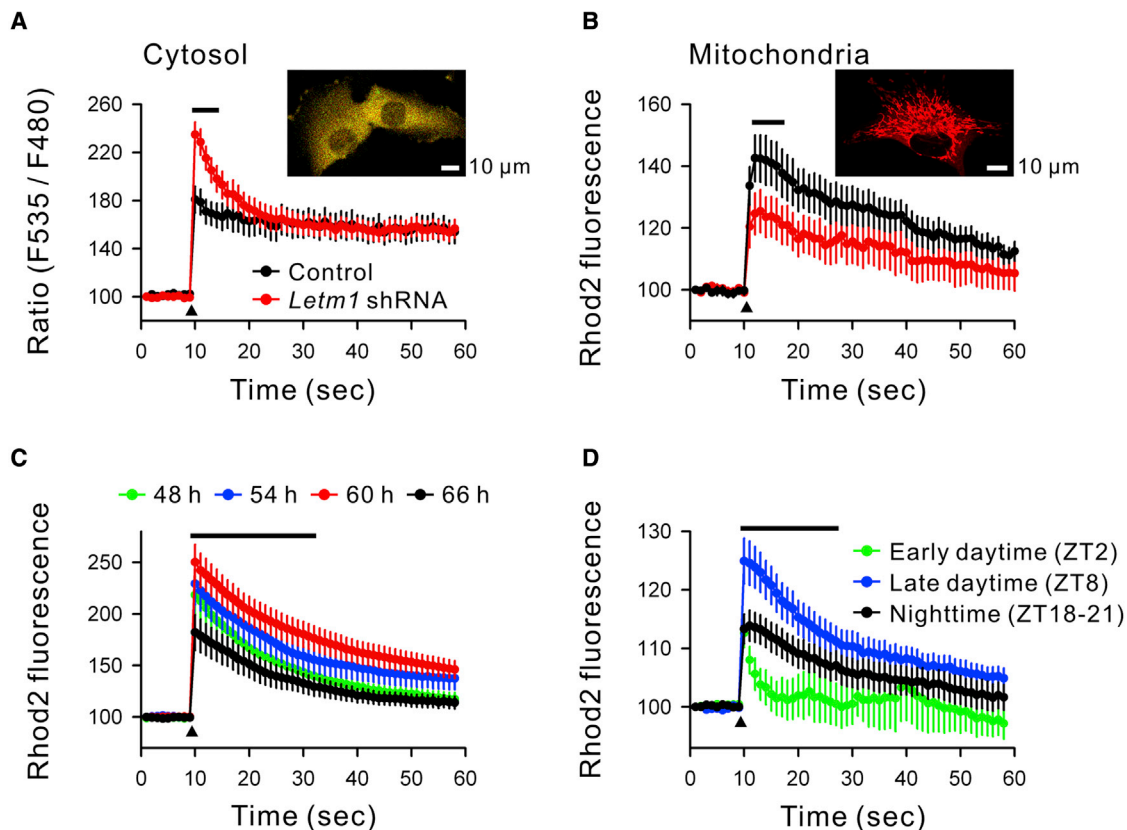


Figure 7. Circadian rhythms in mitochondrial Ca^{2+} uptake in model cells and rat SCN neurons

(A) Effects of *Letm1* knockdown on cytosolic Ca^{2+} elevations were analyzed using hRPE-YC cells stably transfected with *Letm1* shRNA or scrambled shRNA. For the stimulation, preloaded caged Ca^{2+} probes were un-caged by a blue-violet laser pulse given at the time indicated by the arrowhead. Larger elevation of cytosolic Ca^{2+} concentrations was observed in the *Letm1* knockdown group. Number of cells = 29 for each group. (B) Same experiment as in (A), but mitochondrial Ca^{2+} concentrations were monitored using the Rhod 2 Ca^{2+} sensor. A reduced mitochondrial Ca^{2+} response was observed in the *Letm1* knockdown group. Number of cells = 10–12 for this experiment. (C) Mitochondrial Ca^{2+} response in (B) was analyzed at different time points (48–66 h) after Dex treatment in hRPE-YC cells. Note that the mitochondrial Ca^{2+} response displayed circadian variations. Number of cells = 13–20 per time point. (D) Mitochondrial Ca^{2+} measurements in acutely isolated rat brain slices. Compared with early daytime (ZT2, green circles) and nighttime observations (ZT18–21, black circles), mitochondrial Ca^{2+} elevation was larger during late-daytime observations (ZT8, blue circles) in rat SCN neurons. Number of neurons = 11–23 for each group. Horizontal black bars in (A–D) indicate a statistical difference ($p < 0.05$ by two-way repeated-measures ANOVA followed by Tukey’s post hoc test for individual comparisons).

moderately (–25.2%) reduced ATP synthesis ($p < 0.05$, Student’s t test; Figure 6D). In comparison, mitochondrial morphologies visualized by MitoTracker Red were indistinguishable between the *Letm1* shRNA and control groups (Figure 6B). Using hRPE cells lacking YC3.6 expression, mitochondrial membrane potentials were analyzed by JC-1 staining, which revealed that the JC-1 fluorescence ratio (535 and 590 nm) was also indistinguishable between the *Letm1* shRNA and control groups (Figure S3). Notably, *Bmal1* transcriptional rhythms in hRPE-YC cells after Dex treatment were not significantly influenced by *Letm1* knockdown (Period length: control = 23.4 ± 0.1 , *Letm1* shRNA = 23.8 ± 0.5 , $p = 0.45$, Student’s t test; Figure 6E). Despite the steady oscillations in *Bmal1* transcription, intrinsic *Letm1* mRNA ($p = 0.55$, Kruskal-Wallis test; Figure 6F) and protein expression ($p = 0.82$, one-way ANOVA; Figures 6G, S4, and S5) were not under circadian control in hRPE-YC cells.

To analyze intra-mitochondrial Ca^{2+} responses, hRPE-YC cells were stained with Rhod 2-AM together with NP-EGTA-AM (caged Ca^{2+} compound), and mitochondrial Ca^{2+} uptake following photolytic Ca^{2+} elevation in the cytosol was quantified. To compare cytosolic Ca^{2+} responses, YC3.6 fluorescence was also monitored in these photolytic experiments. Although the absolute intensity of Rhod 2 fluorescence before recordings was variable ($525.9 \pm 53.2/12$ -bit depth imaging), it was not significantly different between the *Letm1* knockdown group and the control group ($p = 0.35$, Student’s t test). We found that cytosolic Ca^{2+} transients were elevated (+66.8% at peak level, $p < 0.05$, two-way repeated-measures ANOVA; Figure 7A), whereas mitochondrial Ca^{2+} transients (i.e., uptakes) were reduced by *Letm1* knockdown (–40.2% at peak level, $p < 0.05$, two-way repeated-measures ANOVA; Figure 7B), confirming that LETM1 functions as a mitochondrial antiporter. Importantly, time-dependent mitochondrial Ca^{2+} uptakes were

observed in hRPE-YC cells after Dex treatment ($p < 0.05$, two-way repeated-measures ANOVA; [Figure 7C](#)). Moreover, circadian rhythms in mitochondrial Ca^{2+} uptake were also observed in rat SCN neurons in acute brain slices, where the largest mitochondrial Ca^{2+} uptake was observed late during the daytime (ZT8) compared with the responses early during the daytime (ZT2) or nighttime (pooled for ZT18–21) ($p < 0.05$, two-way repeated-measures ANOVA; [Figure 7D](#)).

DISCUSSION

In the present study, we demonstrate LETM1-dependent circadian cytosolic H^+ rhythms in *Drosophila* LNs as well as LETM1-dependent circadian cytosolic Ca^{2+} rhythms in rat SCN neurons. LETM1 is localized to the inner mitochondrial membrane and functions as a K^+/H^+ exchanger in *Drosophila* and as a $\text{Ca}^{2+}/\text{H}^+$ exchanger in mammals ([McQuibban et al., 2010](#); [Jiang et al., 2013](#)). Cation transport by LETM1 is coupled to ATP synthesis in mitochondria ([Doonan et al., 2014](#)). Therefore, it is reasonable to hypothesize that bioenergetic activity-coupled ion transport by LETM1 underlies the robust ionic rhythms in circadian pacemaker neurons.

Although analysis of an RNAi series with regard to behavioral rhythms in *Drosophila* indicated involvement of other proton transporters ([Figure S1](#)), the action of *Letm1* RNAi observed in the present study suggests that the essential function of LETM1 involves clock regulation. Additionally, knockdown of *Letm1* prolonged nuclear PER/TIM rhythms in LNs and dampened *Bmal1* transcriptional rhythms in SCN neurons. While *Bmal1* transcriptional rhythmicity was apparent in hRPE-YC cells following Dex treatment, it was not affected by *Letm1* knockdown. Therefore, the effects of *Letm1* knockdown may be specific for circadian pacemaker neurons, although cell type-specific action needs to be analyzed using more diverse cell types. Circadian rhythms in Ca^{2+} -spiking frequencies but not large-amplitude rhythms in steady-state Ca^{2+} concentration levels were detectable in hRPE-YC cells ([Ikarashi et al., 2017](#)). Therefore, we hypothesize that the differential effects of *Letm1* knockdown on *Bmal1* transcriptional rhythms may be due to the presence or absence of ionic feedback machineries in these cells. It has been proposed that high-density neurons in the SCN ([Liu et al., 2007](#); [Leise et al., 2012](#); [Noguchi et al., 2017](#)) and neuronal-glia communication ([Brancaccio et al., 2017, 2019](#); [Myung et al., 2018](#)) contribute network (i.e., cell-to-cell communication)-dependent stable oscillations within the central clock system. Here, we additionally propose an intracellular gear in central pacemaker neurons, comprised of LETM1-driven ionic feedback, for the stabilization of TTFLs.

The present study used YC2.1 to analyze pupal LN cultures but failed to observe circadian FRET during long-term fluorescence monitoring ([Figure 1](#)). This observation, however, does not exclude the presence of cytosolic Ca^{2+} rhythms in *Drosophila* LNs. Indeed, circadian cytosolic Ca^{2+} rhythms have been reported in LNs *in vivo* in adult flies by using YC2.1 and GCaMP6s ([Liang et al., 2016](#)). A simple explanation for this discrepancy is the difference in the developmental stages of LNs used for the experiments. Reported circadian cytosolic Ca^{2+} rhythms in LNs *in vivo* ([Liang et al., 2016](#)) could be driven

by mature synaptic interactions and neuronal depolarization (i.e., possibly via TTX-sensitive/voltage-dependent mechanisms). Alternatively, immature LNs might not possess the intracellular machinery to generate circadian cytosolic Ca^{2+} rhythms. Lack of apparent circadian rhythms in cytosolic Ca^{2+} concentrations has been found in SCN progenitor cells ([Takeuchi et al., 2014](#)), supporting this hypothesis. Furthermore, we should note the technical difficulties in sensing Ca^{2+} with GFP-based Ca^{2+} sensors in LNs, because most are acid sensitive, including GCaMP family members (personal communication with Prof. Junichi Nakai, Tohoku University, the GCaMP designer). Therefore, we recommend further analysis of circadian cytosolic Ca^{2+} rhythms in *Drosophila* LNs by developing sensors based on acid-tolerant fluorescent proteins ([Shinoda et al., 2018](#)).

Action potential firings in large LN_vs have been reported to be high during the day and low during the night ([Cao and Nitabach, 2008](#); [Sheeba et al., 2008](#)). The pH-dependent curve demonstrates significant reduction in action potential firing frequencies at low pH ranges ([Figure 2](#)). Therefore, nighttime acidosis of LNs observed in the present study may account for the silence of these neurons during the nighttime. It has been reported that specific types of voltage-sensitive K^+ channels (Shaw Kv3 and Shal Kv4) control circadian changes in action potential firing in LN_vs ([Smith et al., 2019](#)). Acid (pH 6.0–7.0) inactivation has been reported in Kv3 families ([Abbott et al., 2006](#)); thus, it is reasonable to hypothesize that such pH-sensitive mechanisms link circadian cytosolic H^+ rhythms and action potential firing rhythms in LNs. In this regard, in SCN neurons, the large-conductance Ca^{2+} -sensitive K^+ channel is important for the rhythmic changes in membrane excitability. Indeed, BK mutants alter circadian behavior ([Meredith et al., 2006](#); [Kent and Meredith, 2008](#); [Whitt et al., 2016](#)). Additionally, small-conductance Ca^{2+} -sensitive K^+ channels control the rhythmic firing of clock neurons ([Belle et al., 2009](#)). Thus, LETM1-driven circadian cytosolic Ca^{2+} rhythms could further drive action potential firing rhythms in SCN neurons. The circadian cytosolic Ca^{2+} rhythms are slightly phase advanced relative to firing rhythms ([Ikeda et al., 2003](#); [Ono et al., 2017](#)), supporting this conjecture. Together with the possible pH-dependent regulation of action potential firing rhythms in LNs, we suggest that LETM1-dependent ion transport could be a common ionic rhythm driving physiological output rhythms in circadian pacemaker neurons.

In SCN neurons, circadian FRET was observed with a classical YC2.1 sensor ([Ikeda et al., 2003](#); [Ikeda and Ikeda, 2014](#)) as well as with newer Ca^{2+} sensors in SCN cells ([Enoki et al., 2012](#); [Brancaccio et al., 2013, 2017](#); [Noguchi et al., 2017](#); [Ono et al., 2017](#); [Wu et al., 2018](#)). Circadian cytosolic Ca^{2+} rhythms have been consistently observed in different experimental models including organotypic SCN cultures and dispersed primary cultures of SCN neurons. We have preliminary data from the monitoring of deGFP4 fluorescence in cultured SCN neurons and hRPE cells, but we have so far failed to observe circadian fluctuations in fluorescence (data not shown). Although additional studies in more diverse cell types under different conditions (e.g., *in vitro* and *in vivo*) will be required to verify our hypothesis, these observations suggest that circadian pH-related rhythms, such as in *Drosophila* LNs, are absent in

mammalian cells. The lack of strong fluctuations in cytosolic H^+ in SCN neurons may be due to a stronger pH-buffering system in mammalian neurons; however, we do not exclude the possibility that local H^+ concentrations, such as in axon terminals, fluctuate in parallel with spontaneous firing rhythms. Thus, critical ion(s) driving physiological output rhythms via LETM1 may be species specific.

Our current findings demonstrate that uptake of cytosolic Ca^{2+} into mitochondria display circadian variations in hRPE-YC cells and rat SCN neurons. Peak Ca^{2+} uptake occurred late during the daytime in SCN neurons, consistent with the decline phase of circadian cytosolic Ca^{2+} rhythms (Ikeda et al., 2003). Also, the peak Ca^{2+} uptake in SCN neurons may be in phase with mitochondrial H^+ uptake in LNs because cytosolic pH in LNs was less acidic middle-to-late during the daytime (Figures 3D and 3E). The size of mitochondria is reported to be maximal (i.e., fusion status) at the onset of subjective daytime in fibroblast models (Schmitt et al., 2018; Sardon Puig et al., 2018). Although circadian rhythms in fusion/fission status in SCN neurons are currently unknown, Ca^{2+} uptake capacity may not be simply dependent on the physical size of single mitochondria. Indeed, we did not find apparent circadian variations in mitochondrial morphologies in hRPE cells (Figure S5). Previous reports indicated no or little circadian variation in *Letm1* transcription in the mouse SCN (Pembroke et al., 2015) and hippocampus (Renaud et al., 2015). Consistently, no apparent circadian variations in transcriptional and protein levels of LETM1 were found in hRPE-YC cells in the present study. Nevertheless, mitochondrial Ca^{2+} uptake exhibited apparent circadian variations in hRPE-YC cells. It has been shown that PTEN-induced kinase 1 (PINK1)-mediated phosphorylation of LETM1 (Thr192) regulates Ca^{2+} transport in liposomes and mitochondrial Ca^{2+} transport in mouse cortical neurons (Huang et al., 2017). Recently, sleep phenotypes of *Pink1* mutations in LN_vs have been reported in *Drosophila*, where reduced morning anticipation activities during LD cycles and significant reduction in circadian rhythmicity under DD were observed (Valadas et al., 2018). Thus, it is reasonable to hypothesize that circadian regulation of LETM1 by PINK1 underlies circadian cytosolic H^+ or Ca^{2+} rhythms in pacemaker neurons.

Theoretically, circadian rhythms in steady-state intra-mitochondrial Ca^{2+} concentrations may also account for the circadian variations in the uptake of cytosolic Ca^{2+} into mitochondria. However, we addressed neither circadian rhythms in intra-mitochondrial Ca^{2+} concentrations nor Ca^{2+} release from mitochondria via LETM1. To directly assess intra-mitochondrial Ca^{2+} dynamics in SCN neurons, we examined transfection of the mitochondrial-targeting ratiometric Pericam into murine hypothalamic slice cultures (Ikeda et al., 2005); however, long-term monitoring of intra-mitochondrial ions in SCN neurons was difficult because of the low survival rate of neurons following mitochondrial Pericam expression. In this regard, a recent study by Scrima et al. (2020) used flow cytometric analysis of Rhod 1 in a HepG2 hepatocellular carcinoma cell line and estimated circadian variations in mitochondrial Ca^{2+} contents. Although we did not observe differences in Rhod 2 staining intensities in any experimental groups before photolytic stimulation, it is possible that steady-state intra-mitochondrial Ca^{2+} concentrations

influence the circadian variations in uptake of cytosolic Ca^{2+} into mitochondria.

In SCN neurons, generation of circadian cytosolic Ca^{2+} rhythms was dependent on ER stores because they were reduced by ryanodine and 8-bromo-cyclic ADP ribose (Ikeda et al., 2003). Because cyclic ADP ribose is synthesized from NAD^+ by ADP-ribosyl cyclase, an initial trigger for the cytosolic Ca^{2+} elevation may be associated with cellular metabolic signals. In addition, Scrima et al. (2020) suggested that the mitochondrial Ca^{2+} influx originating from the ER store drives clock gene-dependent activation of pyruvate dehydrogenase and oxidative phosphorylation. Thus, it seems likely that cytosolic Ca^{2+} , mitochondrial Ca^{2+} , and metabolic activities organize feedback loops and strengthen cellular circadian oscillations with TTFLs. The present results support this hypothesis and further suggest that mitochondrial cation transport via LETM1 is critical to drive intrinsic rhythms in cytosolic Ca^{2+} or H^+ concentrations, metabolic activities, and clock gene TTFLs in circadian pacemaker neurons.

LETM1-driven circadian ionic rhythms may feed back to influence TTFLs, as delayed nuclear PER/TIM expression and dampened *Bmal1* transcriptional rhythms are induced by *Letm1* knockdown. Simultaneous monitoring of *Per1-luc* and *Bmal1-Eluc* with GCamp6s in cultured SCNs on an electrode array dish demonstrated a lag time between *Bmal1* transcriptional rhythms and other events including cytosolic Ca^{2+} rhythms (Ono et al., 2017). Consistently, our present results demonstrate a rapid reduction in transcriptional levels of *Bmal1* and progressive dampening of cytosolic Ca^{2+} rhythms by *Letm1* knockdown in SCN neurons. In *Drosophila*, nuclear PER levels were reduced most significantly in large LN_vs, whereas nuclear PER/TIM rhythms were delayed but not diminished in small LN_vs. These results suggest a hierarchy of multiple clock components with differential metabolic and ionic controls, possibly in a species-specific manner. The core circadian clock machinery has been reported to include intermolecular interactions, protein phosphorylation, and transcriptional regulation in and out of the nucleus (Dunlap, 1999; Reppert and Weaver, 2002; Gallego and Virshup, 2007). Unfortunately, neither linkage between the TTFLs and physiological output rhythms nor specific machinery in circadian pacemaker neurons has been described in these models. The present results showing a significant impact of *Letm1* knockdown on clock gene TTFLs in both invertebrates and vertebrates suggests that a more complex framework is required to adequately describe the intracellular clockwork machinery, including relationships to metabolic and ionic rhythms via mitochondria. As described above, mitochondria-ER interactions could be specific to circadian pacemaker neurons; however, the subcellular structures required for the generation of robust circadian rhythms need to be explored in future studies.

LETM1 is often deleted in Wolf-Hirschhorn syndrome (WHS) (Endele et al., 1999; Zollino et al., 2003; Doonan et al., 2014), a disorder caused by deletions of the short arm of chromosome 4, encompassing multiple genes. WHS is associated with severe growth and mental retardation. Sleep disorders have been reported in the early years of childhood in patients with WHS (Battaglia et al., 2001). The Children's Sleep Habits

Questionnaire (parental questionnaire of patients with WHS) also indicates excessive sleepiness during the day and moving during the night in patients with WHS (Nag et al., 2017). Our current findings shed light on the underlying mechanisms, although further studies are needed to clarify the role of LETM1 in human circadian behaviors.

Limitations of the study

Previous work of ours (Ikeda et al., 2003; Ikeda, 2004; Ikeda and Ikeda, 2014) suggested that Ca^{2+} release from ER stores is important for the formation of circadian cytosolic Ca^{2+} rhythms in SCN neurons; thus, together with the present results, it seems likely that mitochondria-ER interactions are critical for the formation of autonomous intracellular ionic rhythms in circadian pacemaker neurons. However, there is currently no direct evidence that Ca^{2+} storage within the organelle has an antiphase rhythm to the cytosolic Ca^{2+} rhythm. To obtain experimental proof of this, it will be necessary to develop a technique that can stably monitor ionic rhythm in each organelle over a long period of time and with 3D spatial resolution. In addition, the present study suggests that the LETM1-mediated stabilization of clock gene transcription rhythms is likely to be a phenomenon specific to circadian pacemaker neurons. This is a notable claim of this study because there have been no reports showing intracellular mechanisms specific to such neurons. However, future verification using more diverse cell types is needed to prove this hypothesis.

STAR★METHODS

Detailed methods are provided in the online version of this paper and include the following:

- KEY RESOURCES TABLE
- RESOURCE AVAILABILITY
 - Lead contact
 - Material availability
 - Data and code availability
- EXPERIMENTAL MODEL AND SUBJECT DETAILS
 - *Drosophila* stocks
 - Rats
 - hRPE cell culture and gene transfection
- METHOD DETAILS
 - Organotypic cultures of *Drosophila* central nervous system (CNS)
 - Calcium and pH imaging in *Drosophila* neurons
 - Electrophysiology of *Drosophila* neurons
 - Locomotor activity assay
 - Anti-PER and TIM immunohistochemistry
 - Real-time RT-PCR assay
 - *Bmal1-luc* chemiluminescence counting in model cells
 - Western blotting
 - Anti-LETM1 immunocytochemistry
 - ATP assay
 - Calcium imaging in hRPE-YC cells
 - Calcium imaging of rat SCN neurons in acute brain slices
 - Organotypic SCN cultures

- Co-transfection of YC3.6, *Bmal1-luc* and *Letm1* shRNA into cultured SCN neurons
- Long-term calcium imaging in cultured SCN neurons
- *Bmal1-luc* imaging in cultured SCN neurons
- Mitochondrial membrane potential assay
- QUANTIFICATION AND STATISTICAL ANALYSIS

SUPPLEMENTAL INFORMATION

Supplemental information can be found online at <https://doi.org/10.1016/j.celrep.2022.110787>.

ACKNOWLEDGMENTS

This work was supported in part by JSPS KAKENHI grant number JP16H04651 to E.M. Masaaki Ikeda, and Masayuki Ikeda; JP18K19330 to E.M. and Masayuki Ikeda; and JP15H06232-JP19K16185 to E.M. This work was also supported by the Naito Foundation to E.M., NIH grant R35GM127102 to T.C.H., and JST Moonshot R&D grant JPMJMS2021 to University of Toyama. We thank Keita Koizumi (Kanazawa University) and S. James Remington (University of Oregon) for technical support with deGFP4 experiments. We thank Tomoko Onishi, Nozomi Murayama, and Daisuke Miyake for help with the photolysis experiments, Risa Miyajima for help with PCR assays, and Mari Nagase for performing immunostaining assays.

Q9

AUTHOR CONTRIBUTIONS

E.M., Y. Kasuga, Y. Kanda, S.M., H.K., and N.M. performed experiments. E.M. designed the study and analyzed the data. Masaaki Ikeda, T.Y., and H.H. supplied experimental materials and supervised transgene experiments in flies and rats. T.C.H. and Masayuki Ikeda organized the project and wrote the paper.

DECLARATION OF INTERESTS

The authors declare no competing interests.

Received: January 13, 2021

Revised: March 14, 2022

Accepted: April 14, 2022

Published: May 10, 2022

REFERENCES

- Abbott, G.W., Butler, M.H., and Goldstein, S.A.N. (2006). Phosphorylation and protonation of neighboring MiRP2 sites: function and pathophysiology of MiRP2-Kv3.4 potassium channels in periodic paralysis. *FASEB J.* 20, 293–301. <https://doi.org/10.1096/fj.05-5070com>.
- Abe, M., Herzog, E.D., Yamazaki, S., Straume, M., Tei, H., Sakaki, Y., Menaker, M., and Block, G.D. (2002). Circadian rhythms in isolated brain regions. *J. Neurosci.* 22, 350–356. <https://doi.org/10.1523/JNEUROSCI.22-01-00350.2002>.
- Balsalobre, A., Damiola, F., and Schibler, U. (1998). A serum shock induces circadian gene expression in mammalian tissue culture cells. *Cell* 93, 929–937. [https://doi.org/10.1016/s0092-8674\(00\)81199-x](https://doi.org/10.1016/s0092-8674(00)81199-x).
- Battaglia, A., Carey, J.C., and Wright, T.J. (2001). Wolf-Hirschhorn (4p-) syndrome. *Adv. Pediatr.* 48, 75–113.
- Belle, M.D.C., Diekman, C.O., Forger, D.B., and Piggins, H.D. (2009). Daily electrical silencing in the mammalian circadian clock. *Science* 326, 281–284. <https://doi.org/10.1126/science.1169657>.
- Bernardi, P. (1999). Mitochondrial transport of cations: channels, exchangers, and permeability transition. *Physiol. Rev.* 79, 1127–1155. <https://doi.org/10.1152/physrev.1999.79.4.1127>.
- Brancaccio, M., Patton, A.P., Chesham, J.E., Maywood, E.S., and Hastings, M.H. (2017). Astrocytes control circadian timekeeping in the suprachiasmatic

- nucleus via glutamatergic signaling. *Neuron* 93, 1420–1435.e5. <https://doi.org/10.1016/j.neuron.2017.02.030>.
- Brancaccio, M., Edwards, M.D., Patton, A.P., Smyllie, N.J., Chesham, J.E., Maywood, E.S., and Hastings, M.H. (2019). Cell-autonomous clock of astrocytes drives circadian behavior in mammals. *Science* 363, 187–192. <https://doi.org/10.1126/science.aat4104>.
- Brancaccio, M., Maywood, E.S., Chesham, J.E., Loudon, A.S., and Hastings, M.H. (2013). A Gq-Ca²⁺ axis controls circuit-level encoding of circadian time in the suprachiasmatic nucleus. *Neuron* 78, 714–728. <https://doi.org/10.1016/j.neuron.2013.03.011>.
- Cao, G., and Nitabach, M.N. (2008). Circadian control of membrane excitability in *Drosophila melanogaster* lateral ventral clock neurons. *J. Neurosci.* 28, 6493–6501. <https://doi.org/10.1523/JNEUROSCI.1503-08.2008>.
- Doonan, P.J., Chandramoorthy, H.C., Hoffman, N.E., Zhang, X., Cárdenas, C., Shanmughapriya, S., Rajan, S., Vallem, S., Chen, X., Foskett, J.K., et al. (2014). LETM1-dependent mitochondrial Ca²⁺ flux modulates cellular bioenergetics and proliferation. *FASEB J.* 28, 4936–4949. <https://doi.org/10.1096/fj.14-256453>.
- Dunlap, J.C. (1999). Molecular bases for circadian clocks. *Cell* 96, 271–290. [https://doi.org/10.1016/S0092-8674\(00\)80566-8](https://doi.org/10.1016/S0092-8674(00)80566-8).
- Edgar, R.S., Green, E.W., Zhao, Y., van Ooijen, G., Olmedo, M., Qin, X., Xu, Y., Pan, M., Valekunja, U.K., Feeney, K.A., et al. (2012). Peroxiredoxins are conserved markers of circadian rhythms. *Nature* 485, 459–464. <https://doi.org/10.1038/nature11088>.
- Endele, S., Fuhry, M., Pak, S.J., Zabel, B.U., and Winterpacht, A. (1999). LETM1, a novel gene encoding a putative EF-hand Ca²⁺-binding protein, flanks the Wolf-Hirschhorn syndrome (WHS) critical region and is deleted in most WHS patients. *Genomics* 60, 218–225. <https://doi.org/10.1006/geno.1999.5881>.
- Enoki, R., Kuroda, S., Ono, D., Hasan, M.T., Ueda, T., Honma, S., and Honma, K.i. (2012). Topological specificity and hierarchical network of the circadian calcium rhythm in the suprachiasmatic nucleus. *Proc. Natl. Acad. Sci. U S A* 109, 21498–21503. <https://doi.org/10.1073/pnas.1214415110>.
- Fogle, K.J., Parson, K.G., Dahm, N.A., and Holmes, T.C. (2011). CRYPTOCHROME is a blue-light sensor that regulates neuronal firing rate. *Science* 331, 1409–1413. <https://doi.org/10.1126/science.1199702>.
- Gallego, M., and Virshup, D.M. (2007). Post-translational modifications regulate the ticking of the circadian clock. *Nat. Rev. Mol. Cell Biol.* 8, 139–148. <https://doi.org/10.1038/nrm2106>.
- Green, D.J., and Gillette, R. (1982). Circadian rhythm of firing rate recorded from single cells in the rat suprachiasmatic brain slice. *Brain Res.* 245, 198–200. [https://doi.org/10.1016/0006-8993\(82\)90361-4](https://doi.org/10.1016/0006-8993(82)90361-4).
- Hanson, G.T., McAnaney, T.B., Park, E.S., Rendell, M.E.P., Yarbrough, D.K., Chu, S., Xi, L., Boxer, S.G., Montrose, M.H., and Remington, S.J. (2002). Green fluorescent protein variants as ratiometric dual emission pH sensors. 1. Structural characterization and preliminary application. *Biochemistry* 41, 15477–15488. <https://doi.org/10.1021/bi026609p>.
- Harrisingh, M.C., and Nitabach, M.N. (2008). Integrating circadian timekeeping with cellular physiology. *Science* 320, 879–880. <https://doi.org/10.1126/science.1158619>.
- Hoyle, N.P., and O'Neill, J.S. (2015). Oxidation-reduction cycles of peroxiredoxin proteins and nontranscriptional aspects of timekeeping. *Biochemistry* 54, 184–193. <https://doi.org/10.1021/bi5008386>.
- Huang, E., Qu, D., Huang, T., Rizzi, N., Boonying, W., Krolak, D., Ciana, P., Woulfe, J., Klein, C., Slack, R.S., et al. (2017). PINK1-mediated phosphorylation of LETM1 regulates mitochondrial calcium transport and protects neurons against mitochondrial stress. *Nat. Commun.* 8, 1399. <https://doi.org/10.1038/s41467-017-01435-1>.
- Ikarashi, R., Akechi, H., Kanda, Y., Ahmad, A., Takeuchi, K., Morioka, E., Sugiyama, T., Ebisawa, T., Ikeda, M., and Ikeda, M. (2017). Regulation of molecular clock oscillations and phagocytic activity via muscarinic Ca²⁺ signaling in human retinal pigment epithelial cells. *Sci. Rep.* 7, 44175. <https://doi.org/10.1038/srep44175>.
- Ikeda, M., and Ikeda, M. (2014). *Bmal1* is an essential regulator for circadian cytosolic Ca²⁺ rhythms in suprachiasmatic nucleus neurons. *J. Neurosci.* 34, 12029–12038. <https://doi.org/10.1523/JNEUROSCI.5158-13.2014>.
- Ikeda, M. (2004). Calcium dynamics and circadian rhythms in suprachiasmatic nucleus neurons. *Neuroscientist* 10, 315–324. <https://doi.org/10.1177/10738584031262149>.
- Ikeda, M., Ikeda-Sagara, M., Okada, T., Clement, P., Urade, Y., Nagai, T., Sugiyama, T., Yoshioka, T., Honda, K., and Inoué, S. (2005). Brain oxidation is an initial process in sleep induction. *Neuroscience* 130, 1029–1040. <https://doi.org/10.1016/j.neuroscience.2004.09.057>.
- Ikeda, M., Sugiyama, T., Wallace, C.S., Gompf, H.S., Yoshioka, T., Miyawaki, A., and Allen, C.N. (2003). Circadian dynamics of cytosolic and nuclear Ca²⁺ in single suprachiasmatic nucleus neurons. *Neuron* 38, 253–263. [https://doi.org/10.1016/S0896-6273\(03\)00164-8](https://doi.org/10.1016/S0896-6273(03)00164-8).
- Jiang, D., Zhao, L., Clish, C.B., and Clapham, D.E. (2013). Letm1, the mitochondrial Ca²⁺/H⁺ antiporter, is essential for normal glucose metabolism and alters brain function in Wolf-Hirschhorn syndrome. *Proc. Natl. Acad. Sci. U S A* 110, E2249–E2254. <https://doi.org/10.1073/pnas.1308558110>.
- Kent, J., and Meredith, A.L. (2008). BK channels regulate spontaneous action potential rhythmicity in the suprachiasmatic nucleus. *PLoS One* 3, e3884. <https://doi.org/10.1371/journal.pone.0003884>.
- Koizumi, K., Higashida, H., Yoo, S., Islam, M.S., Ivanov, A.I., Guo, V., Pozzi, P., Yu, S.H., Rovescalli, A.C., Tang, D., and Nirenberg, M. (2007). RNA interference screen to identify genes required for *Drosophila* embryonic nervous system development. *Proc. Natl. Acad. Sci. U S A* 104, 5626–5631. <https://doi.org/10.1073/pnas.0611687104>.
- Lamia, K.A., Sachdeva, U.M., DiTacchio, L., Williams, E.C., Alvarez, J.G., Egan, D.F., Vasquez, D.S., Juguilon, H., Panda, S., Shaw, R.J., et al. (2009). AMPK regulates the circadian clock by cryptochrome phosphorylation and degradation. *Science* 326, 437–440. <https://doi.org/10.1126/science.1172156>.
- Leise, T.L., Wang, C.W., Gitis, P.J., and Welsh, D.K. (2012). Persistent cell-autonomous circadian oscillations in fibroblasts revealed by six-week single-cell imaging of PER2::LUC bioluminescence. *PLoS One* 7, e33334. <https://doi.org/10.1371/journal.pone.0033334>.
- Liang, X., Holy, T.E., and Taghert, P.H. (2016). Synchronous *Drosophila* circadian pacemakers display nonsynchronous Ca²⁺ rhythms in vivo. *Science* 351, 976–981. <https://doi.org/10.1126/science.aad3997>.
- Liu, A.C., Welsh, D.K., Ko, C.H., Tran, H.G., Zhang, E.E., Priest, A.A., Buhr, E.D., Singer, O., Meeker, K., Verma, I.M., et al. (2007). Intercellular coupling confers robustness against mutations in the SCN circadian clock network. *Cell* 129, 605–616. <https://doi.org/10.1016/j.cell.2007.02.047>.
- Marcheva, B., Ramsey, K.M., Peek, C.B., Affinati, A., Maury, E., and Bass, J. (2013). Circadian clocks and metabolism. *Handb. Exp. Pharmacol.* 217, 127–155. https://doi.org/10.1007/978-3-642-25950-0_6.
- McQuibban, A.G., Joza, N., Meghian, A., Scorzeto, M., Zanini, D., Reipert, S., Richter, C., Schweyen, R.J., and Nowikovsky, K. (2010). A *Drosophila* mutant of LETM1, a candidate gene for seizures in Wolf-Hirschhorn syndrome. *Hum. Mol. Genet.* 19, 987–1000. <https://doi.org/10.1093/hmg/ddp563>.
- Meredith, A.L., Wiler, S.W., Miller, B.H., Takahashi, J.S., Fodor, A.A., Ruby, N.F., and Aldrich, R.W. (2006). BK calcium-activated potassium channels regulate circadian behavioral rhythms and pacemaker output. *Nat. Neurosci.* 9, 1041–1049. <https://doi.org/10.1038/nn1740>.
- Miyawaki, A., Griesbeck, O., Heim, R., and Tsien, R.Y. (1999). Dynamic and quantitative Ca²⁺ measurements using improved cameleons. *Proc. Natl. Acad. Sci. U S A* 96, 2135–2140. <https://doi.org/10.1073/pnas.96.5.2135>.
- Mohawk, J.A., Green, C.B., and Takahashi, J.S. (2012). Central and peripheral circadian clocks in mammals. *Annu. Rev. Neurosci.* 35, 445–462. <https://doi.org/10.1146/annurev-neuro-060909-153128>.
- Moore, R.Y., and Eichler, V.B. (1972). Loss of a circadian adrenal corticosterone rhythm following suprachiasmatic lesions in the rat. *Brain Res.* 42, 201–206. [https://doi.org/10.1016/0006-8993\(72\)90054-6](https://doi.org/10.1016/0006-8993(72)90054-6).

- Morioka, E., Matsumoto, A., and Ikeda, M. (2012). Neuronal influence on peripheral circadian oscillators in pupal *Drosophila* prothoracic glands. *Nat. Commun.* 3, 909. <https://doi.org/10.1038/ncomms1922>.
- Myung, J., Schmal, C., Hong, S., Tsukizawa, Y., Rose, P., Zhang, Y., Holtzman, M.J., De Schutter, E., Herzog, H., Bordyugov, G., and Takumi, T. (2018). The choroid plexus is an important circadian clock component. *Nat. Commun.* 9, 1062. <https://doi.org/10.1038/s41467-018-03507-2>.
- Nag, H.E., Bergsaker, D.K., Hunn, B.S., Schmidt, S., and Hoxmark, L.B. (2017). A structured assessment of motor function, behavior, and communication in patients with Wolf-Hirschhorn syndrome. *Eur. J. Med. Genet.* 60, 610–617. <https://doi.org/10.1016/j.ejmg.2017.08.013>.
- Nakahata, Y., Kaluzova, M., Grimaldi, B., Sahar, S., Hirayama, J., Chen, D., Guarente, L.P., and Sassone-Corsi, P. (2008). The NAD⁺-dependent deacetylase SIRT1 modulates CLOCK-mediated chromatin remodeling and circadian control. *Cell* 134, 329–340. <https://doi.org/10.1016/j.cell.2008.07.002>.
- Noguchi, T., Leise, T.L., Kingsbury, N.J., Diemer, T., Wang, L.L., Henson, M.A., and Welsh, D.K. (2017). Calcium circadian rhythmicity in the suprachiasmatic nucleus: cell autonomy and network modulation. *eNeuro* 4, ENEURO.0160-17.2017. <https://doi.org/10.1523/eneuro.0160-17.2017>.
- O'Neill, J.S., and Reddy, A.B. (2011). Circadian clocks in human red blood cells. *Nature* 469, 498–503. <https://doi.org/10.1038/nature09702>.
- Ono, D., Honma, S., Nakajima, Y., Kuroda, S., Enoki, R., and Honma, K.I. (2017). Dissociation of *Per1* and *Bmal1* circadian rhythms in the suprachiasmatic nucleus in parallel with behavioral outputs. *Proc. Natl. Acad. Sci. U S A* 114, E3699–E3708. <https://doi.org/10.1073/pnas.1613374114>.
- Patch, C.L., Green, C.B., and Takahashi, J.S. (2014). Molecular architecture of the mammalian circadian clock. *Trends Cell Biol.* 24, 90–99. <https://doi.org/10.1016/j.tcb.2013.07.002>.
- Patterson, G.H., Knobel, S.M., Sharif, W.D., Kain, S.R., and Piston, D.W. (1997). Use of the green fluorescent protein and its mutants in quantitative fluorescence microscopy. *Biophys. J.* 73, 2782–2790. [https://doi.org/10.1016/S0006-3495\(97\)78307-3](https://doi.org/10.1016/S0006-3495(97)78307-3).
- Pembroke, W.G., Babbs, A., Davies, K.E., Ponting, C.P., and Oliver, P.L. (2015). Temporal transcriptomics suggest that twin-peaking genes reset the clock. *Elife* 4, e10518. <https://doi.org/10.7554/eLife.10518>.
- Ramsey, K.M., Yoshino, J., Brace, C.S., Abrassart, D., Kobayashi, Y., Marcheva, B., Hong, H.K., Chong, J.L., Buhr, E.D., Lee, C., et al. (2009). Circadian clock feedback cycle through NAMPT-mediated NAD⁺ biosynthesis. *Science* 324, 651–654. <https://doi.org/10.1126/science.1171641>.
- Reinke, H., and Asher, G. (2019). Crosstalk between metabolism and circadian clocks. *Nat. Rev. Mol. Cell Biol.* 20, 227–241. <https://doi.org/10.1038/s41580-018-0096-9>.
- Renaud, J., Dumont, F., Khelifaoui, M., Foisset, S.R., Letourneur, F., Bienvenu, T., Khwaja, O., Dorseuil, O., and Billuart, P. (2015). Identification of intellectual disability genes showing circadian clock-dependent expression in the mouse hippocampus. *Neuroscience* 308, 11–50. <https://doi.org/10.1016/j.neurosci.2015.08.066>.
- Reppert, S.M., and Weaver, D.R. (2002). Coordination of circadian timing in mammals. *Nature* 418, 935–941. <https://doi.org/10.1038/nature00965>.
- Rutter, J., Reick, M., Wu, L.C., and McKnight, S.L. (2001). Regulation of clock and NPAS2 DNA binding by the redox state of NAD cofactors. *Science* 293, 510–514. <https://doi.org/10.1126/science.1060698>.
- Sardon Puig, L., Valera-Alberni, M., Cantó, C., and Pilon, N.J. (2018). Circadian rhythms and mitochondria: connecting the dots. *Front. Genet.* 9, 452. <https://doi.org/10.3389/fgene.2018.00452>.
- Schmitt, K., Grimm, A., Dallmann, R., Oettinghaus, B., Restelli, L.M., Witzig, M., Ishihara, N., Mihara, K., Ripperger, J.A., Albrecht, U., et al. (2018). Circadian control of DRP1 activity regulates mitochondrial dynamics and bioenergetics. *Cell Metab.* 27, 657–666.e5. <https://doi.org/10.1016/j.cmet.2018.01.011>.
- Scrima, R., Cela, O., Agriesti, F., Piccoli, C., Tataranni, T., Pacelli, C., Mazzoccoli, G., and Capitanio, N. (2020). Mitochondrial calcium drives clock gene-dependent activation of pyruvate dehydrogenase and of oxidative phosphorylation. *Biochim. Biophys. Acta Mol. Cell Res.* 1867, 118815. <https://doi.org/10.1016/j.bbamcr.2020.118815>.
- Sheeba, V., Fogle, K.J., Kaneko, M., Rashid, S., Chou, Y.T., Sharma, V.K., and Holmes, T.C. (2008). Large ventral lateral neurons modulate arousal and sleep in *Drosophila*. *Curr. Biol.* 18, 1537–1545. <https://doi.org/10.1016/j.cub.2008.08.033>.
- Shinoda, H., Ma, Y., Nakashima, R., Sakurai, K., Matsuda, T., and Nagai, T. (2018). Acid-tolerant monomeric GFP from *Oligindias formosa*. *Cell Chem. Biol.* 25, 330–338.e7. <https://doi.org/10.1016/j.chembiol.2017.12.005>.
- Smith, P., Buhl, E., Tsaneva-Atanasova, K., and Hodge, J.J.L. (2019). Shaw and Shal voltage-gated potassium channels mediate circadian changes in *Drosophila* clock neuron excitability. *J. Physiol.* 597, 5707–5722. <https://doi.org/10.1113/JP278826>.
- Stephan, F.K., and Zucker, I. (1972). Circadian rhythms in drinking behavior and locomotor activity of rats are eliminated by hypothalamic lesions. *Proc. Natl. Acad. Sci. U S A* 69, 1583–1586. <https://doi.org/10.1073/pnas.69.6.1583>.
- Takeuchi, K., Mohammad, S., Ozaki, T., Morioka, E., Kawaguchi, K., Kim, J., Jeong, B., Hong, J.H., Lee, K.J., and Ikeda, M. (2014). Serotonin-2C receptor involved serotonin-induced Ca²⁺ mobilisations in neuronal progenitors and neurons in rat suprachiasmatic nucleus. *Sci. Rep.* 4, 4106. <https://doi.org/10.1038/srep04106>.
- Thomas, J.A., Buchsbaum, R.N., Zimniak, A., and Racker, E. (1979). Intracellular pH measurements in Ehrlich ascites tumor cells utilizing spectroscopic probes generated in situ. *Biochemistry* 18, 2210–2218. <https://doi.org/10.1021/bi00578a012>.
- Valadas, J.S., Esposito, G., Vandekerckhove, D., Miskiewicz, K., Deaulmerie, L., Raitano, S., Seibler, P., Klein, C., and Verstreken, P. (2018). ER lipid defects in neuropeptidergic neurons impair sleep patterns in Parkinson's disease. *Neuron* 98, 1155–1169.e6. <https://doi.org/10.1016/j.neuron.2018.05.022>.
- Versteven, M., Ernst, K.M., and Stanewsky, R. (2020). A robust and self-sustained peripheral circadian oscillator reveals differences in temperature compensation properties with central brain clocks. *iScience* 23, 101388. <https://doi.org/10.1016/j.isci.2020.101388>.
- Wachter, R.M., King, B.A., Heim, R., Kallio, K., Tsien, R.Y., Boxer, S.G., and Remington, S.J. (1997). Crystal structure and photodynamic behavior of the blue emission variant Y66H/Y145F of green fluorescent protein. *Biochemistry* 36, 9759–9765. <https://doi.org/10.1021/bi970563w>.
- Waldeck-Weiermair, M., Jean-Quartier, C., Rost, R., Khan, M.J., Vishnu, N., Bondarenko, A.I., Imamura, H., Malli, R., and Graier, W.F. (2011). Leucine zipper EF hand-containing transmembrane protein 1 (Letm1) and uncoupling proteins 2 and 3 (UCP2/3) contribute to two distinct mitochondrial Ca²⁺ uptake pathways. *J. Biol. Chem.* 286, 28444–28455. <https://doi.org/10.1074/jbc.M111.244517>.
- Welsh, D.K., Logothetis, D.E., Meister, M., and Reppert, S.M. (1995). Individual neurons dissociated from rat suprachiasmatic nucleus express independently phased circadian firing rhythms. *Neuron* 14, 697–706. [https://doi.org/10.1016/0896-6273\(95\)90214-7](https://doi.org/10.1016/0896-6273(95)90214-7).
- Whitt, J.P., Montgomery, J.R., and Meredith, A.L. (2016). BK channel inactivation gates daytime excitability in the circadian clock. *Nat. Commun.* 7, 10837. <https://doi.org/10.1038/ncomms10837>.
- Wu, Y.E., Enoki, R., Oda, Y., Huang, Z.L., Honma, K.I., and Honma, S. (2018). Ultradian calcium rhythms in the paraventricular nucleus and subparaventricular zone in the hypothalamus. *Proc. Natl. Acad. Sci. U S A* 115, E9469–E9478. <https://doi.org/10.1073/pnas.1804300115>.
- Yamazaki, S., Numano, R., Abe, M., Hida, A., Takahashi, R.I., Ueda, M., Block, G.D., Sakaki, Y., Menaker, M., and Tei, H. (2000). Resetting central and peripheral circadian oscillators in transgenic rats. *Science* 288, 682–685. <https://doi.org/10.1126/science.288.5466.682>.
- Yu, W., Nomura, M., and Ikeda, M. (2002). Interactivating feedback loops within the mammalian clock: BMAL1 is negatively autoregulated and

upregulated by CRY1, CRY2, and PER2. *Biochem. Biophys. Res. Commun.* 290, 933–941. <https://doi.org/10.1006/bbrc.2001.6300>.

Zollino, M., Lecce, R., Fischetto, R., Murdolo, M., Faravelli, F., Selicorni, A., Buttè, C., Memo, L., Capovilla, G., and Neri, G. (2003). Mapping the Wolf-Hirschhorn syndrome phenotype outside the currently accepted WHS critical

region and defining a new critical region, WHSCR-2. *Am. J. Hum. Genet.* 72, 590–597. <https://doi.org/10.1086/367925>.

Zylka, M.J., Shearman, L.P., Weaver, D.R., and Reppert, S.M. (1998). Three *period* homologs in mammals: differential light responses in the suprachiasmatic circadian clock and oscillating transcripts outside of brain. *Neuron* 20, 1103–1110. [https://doi.org/10.1016/s0896-6273\(00\)80492-4](https://doi.org/10.1016/s0896-6273(00)80492-4).

Q5 Q6 STAR★METHODS

KEY RESOURCES TABLE

REAGENT or RESOURCE	SOURCE	IDENTIFIER
Antibodies		
Rabbit anti-Drosophila PER	Chemicon, Temecula, CA, USA	Cat#AB5432P; RRID: AB_91856
Guinea Pig anti-Drosophila TIM39	Laboratory of Jaga Giebultowicz, Oregon State University	N/A
Donkey anti-Rabbit IgG - Cy3	Jackson ImmunoResearch, West Grove, PA, USA	Cat#711-165-152; RRID: AB_2307443
Donkey anti-Guinea Pig IgG – Cy5	Jackson ImmunoResearch	Cat#706-175-148; RRID: AB_2340462
Mouse anti-LETM1 monoclonal antibody (M03), clone 6F7	Abnova Corporation, Taipei City, Taiwan	Cat#H00003954-M03; RRID: AB_534913
Mouse anti-TOMM20 (F-10) monoclonal antibody	Santa Cruz Biotechnology, Dallas, TX, USA	Cat#sc-17764; AB_628381
Donkey anti-mouse IgG - Peroxidase	Jackson ImmunoResearch	Cat#715-035-151; AB_2430771
Donkey anti-Mouse IgG – Alexa Fluor®647	Jackson ImmunoResearch	Cat#115-607-003; RRID: AB_2338931
Chemicals, peptides, and recombinant proteins		
Puromycin	Nacalai Tesque, Kyoto, Japan	Cat#29455-54
Schneider's Drosophila Medium	Gibco, Carlsbad, CA, USA	Cat#21720024
Insulin	Sigma-Aldrich, St Louis, MO, USA	Cat#I1882
Amphotericin B	Invitrogen, Carlsbad, CA, USA	Cat#15290018
(±)-Nicotine	Sigma-Aldrich	Cat#N0267
Propionic acid	Wako Pure Chemical Industries, Osaka, Japan	Cat#163-04726
CCCP: Carbonyl cyanide 3-chlorophenylhydrazone	Sigma-Aldrich	Cat#C2759
Potassium D-gluconate	Sigma-Aldrich	Cat#G4500
Nigericin	Wako Pure Chemical Industries	Cat#145-07263
EGTA	Sigma-Aldrich	Cat#E4378
Paraformaldehyde	Wako Pure Chemical Industries	Cat#162-16065
Normal donkey serum	Jackson ImmunoResearch	Cat#017-000-121
Triton X-100	Sigma-Aldrich	Cat#T9284
Glycerol	Wako Pure Chemical Industries	Cat#075-00616
Beetle luciferin	Promega, Madison, WI, USA	Cat#E1602
Dex: Dexamethasone	Sigma-Aldrich	Cat#D4902
Protease Inhibitor Cocktail for Use with Mammalian Cell and Tissue Extracts	Nacalai Tesque	Cat#25955-24
MitoTracker Red™ CMXRos	ThermoFisher Scientific, Waltham, MA, USA	Cat#M7512
Vectashield mounting medium with DAPI	Vector Laboratories, Burlingame, CA, USA	Cat#H-1200
2.5% Trypsin	Invitrogen	Cat#15090-046
NP-EGTA AM	Molecular Probes, Eugene, OR, USA	Cat#N6803
Rhod 2-AM	Dojindo Laboratories, Kumamoto, Japan	Cat#R002
Pentobarbital Sodium Salt	Tokyo Chemical Industry, Tokyo, Japan	Cat#P0776
Cremophor EL	Nacalai Tesque	Cat# 09727-14
Tetrodotoxin	Wako Pure Chemical Industries	Cat#207-15901
Nimodipine	Sigma-Aldrich	Cat#N149

(Continued on next page)

Continued

REAGENT or RESOURCE	SOURCE	IDENTIFIER
Horse serum	Lonza, Basel, Switzerland	Cat#14-403F
GlutaMAX	Gibco	Cat#35050061
Kanamycin	Invitrogen	Cat#15160054
EDTA	Sigma-Aldrich	Cat#E5513
Spermidine	Sigma-Aldrich	Cat#S2626
JC-1 Dye: 5,5',6,6'-tetrachloro-1,1',3,3'-tetraethylbenzimidazolylcarbocyanine iodide	Molecular Probes	Cat#T3168
FCCP: Carbonylcyanide-4-(trifluoromethoxy)-phenylhydrazone	Enzo Life Sciences, Inc., Farmingdale, NY, USA	Cat#BML-CM120-0010
Critical commercial assays		
Lipofectamine 2000	Thermo Fisher Scientific	Cat#11668-019
Drosophila activity monitor	Trikinetics Inc., Waltham, MA, USA	Cat#DAM2
NucleoSpin® RNA Plus	Takara Bio Inc., Shiga, Japan	Cat#U0984A
RNeasy Mini Kit	Qiagen, Hilden, Germany	Cat#74104
QuantiTect Reverse Transcription Kit	Qiagen	Cat#205311
Rotor-Gene SYBR Green PCR Kit	Qiagen	Cat#204074
Mitochondria Isolation Kit for Cultured Cells	Abcam, Cambridge, UK	Cat#ab110170
Protein Assay BCA Kit	Nacalai Tesque	Cat#06385-00
10% Mini-PROTEAN TGX Precast Protein Gels, 10 well	Bio-Rad Laboratories Inc., Hercules, CA, USA	Cat#4561031
Immobilon-P PVDF Membrane, 0.45 m, 810 cm	Merck Millipore, Darmstadt, Germany	Cat# IPVH08100
Chemi-Lumi One L	Nacalai Tesque	Cat#07880-70
AMERIC-ATP Kit	Applied Medical Enzyme Research Ins. Co., Tokushima, Japan	Cat#AT001
Experimental models: Cell lines		
Human: RPE-YC cell	Ikarashi et al., 2017	N/A
Experimental models: Organisms/strains		
Drosophila: yw; tim-Gal4	Bloomington Drosophila Stock Center, Indiana University, Bloomington, IN, USA	BDRC: 7126
Drosophila: Pdf-Gal4, yw	Bloomington Drosophila Stock Center	BDSC: 6899
Drosophila: w; UAS-Cameleon2.1-82	Bloomington Drosophila Stock Center	BDSC: 6901
Drosophila: elav-Gal4	Bloomington Drosophila Stock Center	BDSC: 8765
Drosophila: w; UAS-deGFP4	This paper	N/A
Drosophila: yw; cry ^b	Laboratory of Akira Matsumoto, Juntendo University	N/A
Drosophila: w; pdfGal4-p12c	Laboratory of Todd C. Holmes, University of California, Irvine (Fogle et al., 2011)	N/A
Drosophila: UAS-Ndae1 ^{RNAi}	Vienna Drosophila Resource Center, Vienna BioCenter Core Facilities, Vienna, Austria	VDRC: 3664
Drosophila: UAS-DmLETM1 ^{RNAi}	Vienna Drosophila Resource Center	VDRC: 6662
Drosophila: UAS-DmNHE1 ^{RNAi}	Vienna Drosophila Resource Center	VDRC: 7245
Drosophila: UAS-Vha100-1 ^{RNAi}	Vienna Drosophila Resource Center	VDRC: 22924
Drosophila: w; UAS-Dicer2	Vienna Drosophila Resource Center	VDRC: 60008
Rat: CrI:CD(SD)	Charles River Laboratories Japan, Inc., Yokohama, Japan	Cat#001A11
Oligonucleotides		
For Primers sequences, see Table S2		N/A

(Continued on next page)

Continued

REAGENT or RESOURCE	SOURCE	IDENTIFIER
Recombinant DNA		
deGFP4	Laboratory of S. James Remington, University of Oregon (Hanson et al., 2002)	FPbase ID: LDZC9
pUAST vector	Laboratory of Akira Matsumoto, Juntendo University	N/A
pNSE/YC3.6	Ikeda and Ikeda, 2014	N/A
Bp/527-Luc	Laboratory of Masaaki Ikeda, Saitama Medical University (Yu et al., 2002)	N/A
RFP-tagged shRNA (Hush, 29-mer shRNA in pRFP-C-RS) against human Letm1 (Locus ID 3954)	OriGene, Rockville, MD, USA	Cat#TF311758A
RFP-tagged scrambled shRNA (Hush, 29-mer scrambled shRNA in pRFP-C-RS) (Locus ID 3954)	OriGene	Cat#TF311758
RFP-tagged shRNA (Hush, 29-mer shRNA in pRFP-C-RS) against rat Letm1 (Locus ID 305457)	OriGene	Cat#TF700692A
Software and algorithms		
Argus-HISCA	Hamamatsu Photonics, Hamamatsu, Japan	N/A
MetaFluor version 6.1 or 7.0	Molecular Devices, San Jose, CA, USA	https://www.moleculardevices.com
pCLAMP 8	Molecular Devices	https://www.moleculardevices.com
DAMSystem3	TriKinetics Inc.	https://trikinetics.com
PACR version 2.0	Written by M.I.	N/A
Photoshop CS 6	Adobe Systems, San Jose, CA, USA	https://www.adobe.com
Rotor-Gene Q series software version 3.2.1	Qiagen	https://www.qiagen.com
NIS-Elements AR4.10	Nikon, Tokyo, Japan	https://www.microscope.healthcare.nikon.com
FV10-ASW	Olympus, Tokyo, Japan	https://www.olympus-lifescience.com
Image Pro Plus 7.0	Media Cybernetics, Rockville, MD, USA	https://www.mediacy.com
MetaMorph version 7.8	Molecular Devices	https://www.moleculardevices.com
BellCurve for Excel	Social Survey Research Information Co., Ltd., Tokyo, Japan	https://bellcurve.jp
SigmaPlot version 7.0	Systat Software Inc., San Jose, CA, USA	http://www.sigmaplot.com
CircWave version 1.4	ClockTool	https://www.clocktool.org
Other		
0.40- μ m Cell Culture Inserts: Millicell	Merck Millipore	Cat#PICM0RG50
0.40- μ m Cell Culture Inserts	BD Falcon, Franklin Lakes, NJ, USA	Cat#353090
Real-time PCR system: Rotor-Gene Q 2plex Platform	Qiagen	Cat#9001620
Multichannel chemiluminescence analyser: Kronos-Dio	ATTO Co. Ltd., Tokyo, Japan	Model: AB-2550
Microplate reader	Hitachi High-Tech Science Corp., Tokyo, Japan	Cat# SH-8100Lab
Vibrating blade tissue slicer	Dosaka em co., Ltd., Kyoto, Japan	Cat#NLS-MT
Helios Gene Gun System	Bio-Rad Laboratories Inc.	Cat#1652431J2

RESOURCE AVAILABILITY

Lead contact

Further information and requests for resources and reagents should be directed to and will be fulfilled by the lead contact, Masayuki Ikeda (msiked@sci.u-toyama.ac.jp).

Material availability

This study did not generate new unique reagents. Fly lines generated in this study are available from the [lead contact](#) with a completed materials transfer agreement.

Data and code availability

All data reported in this paper will be shared by the [lead contact](#) upon request.

This paper does not report original code.

Any additional information required to reanalyze the data reported in this paper is available from the [lead contact](#) upon request.

EXPERIMENTAL MODEL AND SUBJECT DETAILS

Drosophila stocks

Drosophila stocks were maintained on a standard cornmeal-sugar-yeast-agar medium at $25 \pm 1^\circ\text{C}$ under a 12:12-h LD cycle. The *yw*; *tim-Gal4*, *Pdf-Gal4*, *yw*, *w*; *UAS-Cameleon2.1-82* and *elav-Gal4* lines were supplied by the Bloomington Drosophila Stock Center. The *w*; *UAS-deGFP4* line was generated by a standard embryo injection protocol as described previously (Koizumi et al., 2007) in the Haruhiro Higashida laboratory (Kanazawa University). The *cry^b* line was kindly provided by Akira Matsumoto (Juntendo University). The *w*; *pdfGal4-p12c* line (Fogle et al., 2011) was kindly provided by Todd C. Holmes (University of California, Irvine). All RNAi lines (*UAS-Ndae1^{RNAi}*, *UAS-DmLETM1^{RNAi}*, *UAS-DmNHE1^{RNAi}* and *UAS-Vha100-1^{RNAi}*) and the *w*; *UAS-Dicer2* line were obtained from Vienna Drosophila Resource Center RNAi stocks.

Rats

All procedures involving the use of rats were approved by the Institutional Animal Care and Use Committee of the University of Toyama. Sprague–Dawley rats (CrI:CD(SD)) were bred at $24 \pm 1^\circ\text{C}$ under a 12:12-h LD cycle and were used for the following imaging assays. Water and food (regular nutrient co-mixture chow, Labo MR Standard) were available ad libitum.

hRPE cell culture and gene transfection

The hRPE and hRPE-YC cells (Ikarashi et al., 2017) were cultured in Dulbecco's modified Eagle medium/nutrient mixture F-12 supplemented with 10% heat-inactivated fetal bovine serum (FBS), sodium bicarbonate (1.2 g/L) and 1% penicillin/streptomycin at $37 \pm 0.5^\circ\text{C}$ in 5% CO_2 . The cells were transfected with shRNA against human *Letm1* or scrambled shRNA in the pRFP-C-RS vector (Letm1 Human shRNA Plasmid Kit #TF311758) using Lipofectamine 2000. Subsequently, the cells were cultured in medium containing 3 $\mu\text{g}/\text{mL}$ puromycin for cell selection.

METHOD DETAILS

Organotypic cultures of Drosophila central nervous system (CNS)

The preparation and maintenance of organotypic *Drosophila* CNS cultures were as described previously (Morioka et al., 2012). Briefly, CNS cultures were prepared from prepupae 1–3 h after pupariation. Isolated CNS were placed on 0.40- μm culture inserts in 35-mm glass-bottom dishes (glass diameter: 10 mm) or standard 6-well plates and cultured with interface volume (600 μL or 1 mL) of medium comprising 80% Schneider's *Drosophila* medium and 20% (v/v) heat-inactivated FBS, supplemented with 500 ng/mL insulin, 100 units/mL penicillin, 100 $\mu\text{g}/\text{mL}$ streptomycin and 2.5 $\mu\text{g}/\text{mL}$ amphotericin B. The cultures were maintained at $25 \pm 1^\circ\text{C}$ under a LD cycle for 42–66 h prior to recordings.

Calcium and pH imaging in Drosophila neurons

Imaging protocols have been described previously (Morioka et al., 2012). For long-term imaging, YC2.1 or deGFP4 fluorescence from pupal LNs were observed using an upright microscope (Eclipse E600, Nikon, Tokyo, Japan) with an objective lens (LU Plan 50 \times /0.80, Nikon). Ratiometric analysis of YC2.1 was performed by *timeless*-driven YC2.1 expression in pupal LNs. Although the *timeless* driver does not specify expression of YC2.1 in LNs, pupal LNs were visually identified by their anatomical location, cell body size and typical dorsal projection patterns. Ratiometric analysis of deGFP4 was performed by *pdf*-driven deGFP4 expression in pupal LNs. To eliminate excitation light-evoked circadian disruption, *cryptochrome* loss-of-function *cry^b* mutant background flies were used for these experiments. Fluorescent image pairs (YC: 480 ± 15 nm and 535 ± 12.5 nm; deGFP4: 510 ± 20 nm and 465 ± 15 nm) were produced by a 435.8 ± 5 nm or 405 ± 5 nm light pulse (600-ms or 400-ms pulses generated by a 100 W mercury short arc lamp) and reflected using a dichroic mirror (455SPECIAL C68235 or 435DRLP) and an excitation neutral density filter (ND8). Images were acquired using a cooled CCD camera (C4880-80, Hamamatsu Photonics, Hamamatsu, Japan) through a filter changer wheel (M4312, Hamamatsu Photonics) and an electromagnetic shutter (Nidec Copal Electronics, Tokyo, Japan) attached in front of the lamp house. Timings of shutter gating and image acquisitions at 15-sec intervals were regulated by Argus-HiSCA digital imaging software.

For short-term imaging, cultures were cut from a culture insert and transferred to the circulating microscope chamber through which buffered-saline solution, similar to the composition of Schneider's medium, containing (mM) 5.4 CaCl_2 , 21.5 KCl, 15 MgCl_2 , 36 NaCl, 11.1 glucose, 8.3 sucrose and 10 HEPES, was perfused at a flow rate of 1.2 mL/min. YC2.1 or deGFP4 fluorescence

from LNs was observed using an upright microscope (Axioskop 2, Carl Zeiss, Oberkochen, Germany) with a water-immersion objective lens (Achromplan 40 \times /0.75, Carl Zeiss). Fluorescent image pairs (YC: 535 \pm 15 nm and 480 \pm 15 nm; deGFP4: 515 \pm 20 nm and 465 \pm 15 nm) were produced by a 440 \pm 5 nm or 400 \pm 10 nm light pulse (400-ms pulses generated by a 300 W xenon lamp house (Lambda-LS, Sutter Instrument, Novato, CA, USA), which was conducted to the microscope through a liquid light guide and reflected using a dichroic mirror (FT445 nm or FT425 nm). These images were acquired using a cooled CCD camera (CoolSnap Fx, Photometrics, Tucson, AZ, USA) through a filter wheel (Lambda 10-3, Sutter Instrument) attached in front of the camera. Timings of shutter gating and image acquisitions at 6-s intervals were regulated by digital imaging software (MetaFluor ver. 7.0 software; Japan Molecular Devices, Tokyo, Japan). The recording was performed at 24 \pm 1°C. (\pm)-Nicotine, propionic acid or CCCP was applied by switching the perfusate. The CCCP was dissolved in dimethyl sulfoxide and diluted with buffered-saline solution in a final dimethyl sulfoxide concentration of 0.1% (v/v).

The pH calibration in deGFP4 expressed in LNs was performed with pupal CNS cultures using a high-K⁺/nigericin method (Thomas et al., 1979). Cultured samples were superfused with extracellular solution containing (mM) 1.8 CaCl₂, 120 K-gluconate, 0.9 MgCl₂, 5.4 NaCl, 15 glucose, 10 HEPES or MES, and 10 μ M of the proton ionophore nigericin. pH steps in this buffer were adjusted to 6.0–8.5 (0.5 unit) with HCl or NaOH.

Electrophysiology of *Drosophila* neurons

Patch clamp recordings in large-LN_s were performed on acutely dissected whole-brain preparations from adult flies expressing Pdf-driven GFP (*w; pdfGal4-p12c*) as described previously (Sheeba et al., 2008; Fogle et al., 2011). All large-LN_v recordings were performed in whole-cell current clamp mode. The standard external solution contained (mM): 122 NaCl, 3 KCl, 1.8 CaCl₂, 0.8 MgCl₂, 5 glucose, 10 HEPES, pH 7.2–7.3, at 250–255 mOsm. The pipette solution contained (mM): 102 K-gluconate, 17 NaCl, 0.085 CaCl₂, 1.7 MgCl₂, 8.5 HEPES and 0.94 EGTA, adjusted at pH 7.2 and 232–235 mOsm. To analyse the effects of extracellular pH, pH steps (6.0–8.5 adjusted using HCl or NaOH) in external solutions were applied for 4–5 min through the gravity-driven bath perfusion system. All these recordings were performed in Todd C. Holmes's laboratory (University of California, Irvine).

Locomotor activity assay

Locomotor activity monitoring was carried out with 3- to 7-day-old male flies in DAM2 *Drosophila* activity monitors set in a temperature-controlling incubator. Double-plotting actograms and chi-square periodograms of circadian locomotor rhythms were analysed using originally developed software written by M.I. (PACR ver. 2.0). To analyse free-running locomotor rhythms, flies were first entrained in LD cycles for 4 days, then the lighting schedule was switched to DD.

Anti-PER and TIM immunohistochemistry

Anti-PER and TIM immunostaining protocols have been described previously (Morioka et al., 2012). Briefly, adult fly brains were dissected at six different time points on the 4th day under LD or DD conditions. Isolated brains were fixed using 4% (w/v) paraformaldehyde in phosphate-buffered saline (PBS(-)) for 15 min at room temperature. Following three 10-min rinses in PBS(-), brains were then blocked in PBS(-) with 10% (v/v) normal donkey serum and 0.1% (v/v) Triton X-100 overnight at 4°C. Then, brains were incubated for 3–4 days at 4°C with antibodies against *Drosophila* PER (1:1,000) or TIM (1:5,000; Laboratory of Jaga Giebultowicz, Oregon State University). Following three 10-min rinses in PBS(-), samples were incubated with 1:200 Cy3-conjugated donkey anti-rabbit IgG or 1:200 Cy5-conjugated anti-guinea pig IgG for 48 h at 4°C. Following three 10-min rinses in PBS(-), brains were mounted on glass slides and embedded with 80% glycerol. Immunofluorescence images were captured using a confocal laser scanning system (A1R MP plus, Nikon). Optical intensity was analysed using Adobe PhotoShop CS software. The LNs were identified using GFP fluorescence in *pdfGal4-p12c* flies. The boundaries of the nuclei of LNs were defined in the GFP image and superimposed on the PER/TIM image, and then the average intensity of nuclear regions was calculated.

Real-time RT-PCR assay

mRNA was quantified using a real-time RT-PCR system (Rotor-Gene Q series software). To analyse transcriptional levels of *Drosophila Letm1*, total RNA was extracted from five fly brains that expressed *Letm1*^{RNAi} under control of *Elav-Gal4* using NucleoSpin RNA Plus (Takara Bio) in accordance with the manufacturer's instructions. To analyse transcriptional levels of human *Letm1*, total RNA was extracted from hRPE cells cultured in 35-mm dishes at 90% confluency using a NucleoSpin RNA Plus or RNeasy mini kit (Qiagen) as described previously (Ikarashi et al., 2017). cDNA was amplified from 1 μ g of RNA using QuantiTect Reverse Transcription Kit (Qiagen) according to the manufacturer's instructions. The sequences of PCR primers for *Drosophila Letm1* (FlyPrimerBank: PP29077), ribosomal protein 49 (*rp49*), human *Letm1* (Waldeck-Weiermair et al., 2011), *GAPDH* and β -actin are listed in Table S2. Each primer was used with the Rotor-Gene SYBR Green RT-PCR Master Mix in the 72-well rotor of the real-time PCR system (Rotor-Gene Q 2plex Platform). mRNA levels were expressed as 2^{- Δ Ct} using *rp49*, β -actin and *GAPDH* mRNA as internal standard.

Bmal1-luc chemiluminescence counting in model cells

The *Bmal1-luc* rhythms in hRPE-YC cells were analysed as described previously (Ikarashi et al., 2017) using culture medium supplemented with 50 μ M beetle luciferin and a multichannel chemiluminescence analyser (Kronos-Dio, ATTO) set at 37°C. Cells were treated for 1 h with 1 μ M dexamethasone (Dex) and rinsed with fresh culture medium before recordings.

Western blotting

The hRPE-YC cells were cultured on 100-mm dishes to 70–80% confluency, with three dishes ($\sim 1 \times 10^7$ cells) used per condition. Cells were pre-treated for 1 h with 1 μM Dex and cultured with fresh culture medium. Cells were collected by centrifugation at $500 \times g$ for 5 min at different time points after Dex treatment. The mitochondria were isolated using the mitochondrial isolation kit for cultured cells (Abcam, ab110170) according to the manufacturer's instructions. The mitochondrial pellet was resuspended with 50 μL cell lysis buffer comprising 150 mM NaCl, 20 mM Tris-HCl, 1% (w/v) Triton X-100, 10% (w/v) glycerol supplemented with a protease inhibitor cocktail. Total protein concentrations were determined using a standard bicinchoninic acid assay.

For western blotting, mitochondrial proteins were diluted to 2 $\mu\text{g}/\mu\text{L}$ with cell lysis buffer, and mixed with an equal volume of 2 \times SDS sample buffer [125 mM Tris-HCl, 4% (w/v) SDS, 10% (w/v) sucrose, 0.01% (w/v) bromophenol blue, 10% (w/v) 2-mercaptoethanol] and heated at 95°C for 5 min. The solubilized proteins were separated by 10% or 12% sodium dodecyl sulfate–polyacrylamide gel electrophoresis using mini-protean TGX precast gels (Bio-Rad Laboratory). Proteins were transferred onto polyvinylidene fluoride membranes (Immobilon-P PVDF membrane, Merck Millipore) and incubated with 1:5,000 mouse monoclonal antibody against human LETM1 (Abnova) or 1:500 anti-TOMM20 (Santa Cruz) antibodies. The membranes were further incubated with 1:20,000 horseradish peroxidase-conjugated anti-mouse IgG (Jackson ImmunoResearch). Luminol signals were processed with Chemi-Lumi One L (Nacalai Tesque) and acquired using a cooled-CCD gel imaging system (Ez-Capture, ATTO). The optical density of each band was quantified using CS Analyzer software (ATTO).

Anti-LETM1 immunocytochemistry

The hRPE-YC cells were cultured on glass coverslips. Cells were pre-treated for 1 h with 1 μM Dex and cultured with fresh culture medium. Mitochondrial staining was performed with MitoTracker Red CMXRos (75 nM, 15 min) at different time points after Dex treatment. Immediately after the mitochondrial staining, cells were fixed in 4% (w/v) paraformaldehyde in PBS(-) for 15 min at room temperature and washed three times with PBS(-). The fixed cells were then blocked for 2 h at room temperature in PBS(-) with 10% (v/v) normal donkey serum and 0.3% (v/v) Triton X-100. Then, samples were incubated overnight at 4°C on an orbital shaker with 1:200 anti-LETM1 dissolved in PBS(-) with 5% donkey serum and 0.01% Triton X-100. Following three 20-min PBS(-) rinses, samples were incubated with 1:400 Alexa Fluor 647-conjugated donkey anti-mouse IgG for 2 h at room temperature. Following four 15-min PBS(-) rinses on an orbital shaker, samples were mounted on glass slides using VECTASHIELD mounting medium with DAPI. Immunofluorescence images were captured using a confocal laser scanning system (A1R MP plus). Optical intensity was analysed using Image Pro Plus 7.0 software (Media Cybernetics). Mitochondrial LETM1 immunoreactivity levels were normalized as a function of mitochondrial dimension, which was visualized by MitoTracker Red.

ATP assay

Intracellular ATP levels in hRPE-YC cells were measured using a bioluminescence assay kit (AMERIC-ATP Kit) according to the manufacturer's instructions. Cells were seeded onto 25-cm² flasks and cultured as described above in a CO₂ incubator. Cells were grown to 90% confluence and harvested with 0.05% trypsin/0.5 mM EGTA. The resulting cell pellet was resuspended in PBS(-) for ATP extraction and cell counting by haemocytometer to normalize the cell number. Resuspended cells were lysed with the ATP extraction solution provided in the kit and diluted 50-fold with ultrapure water. Following addition of luciferase solution, bioluminescence was immediately measured with a microplate reader. ATP levels in each sample were quantified from the calibration curve.

Calcium imaging in hRPE-YC cells

To monitor cytosolic Ca²⁺, hRPE-YC cells seeded onto 35-mm plastic dishes were grown to 40–60% confluence, and then loaded for 30 min with 5 μM *o*-nitrophenyl-EGTA (NP-EGTA)-AM in a CO₂ incubator. Subsequently, the culture medium was gently rinsed from the dishes using buffered salt solution (BSS) comprising (in mM) 128 NaCl, 5 KCl, 2.7 CaCl₂, 1.2 MgCl₂, 1 Na₂HPO₄, 10 glucose and 10 HEPES (pH 7.3). hRPE-YC cells were placed on a heating stage set at 36°C in an upright confocal laser scanning microscope (A1R MP plus). Fluorescent image pairs (524–550 nm and 465–500 nm) were produced by excitation with a 440-nm diode laser using a 25 \times water-immersion objective lens (Apo LWD 25 \times 1.10w DIC N2, Nikon) and digital imaging software (NIS-Elements AR4.10). The fluorescence images were acquired over a period of 1 min at 1-s intervals. To trigger Ca²⁺ elevation, 405-nm laser stimulation (1 s, spot stimulation) was delivered to the targeted cell.

To monitor mitochondrial Ca²⁺, hRPE-YC cells were loaded for 30 min with 3 μM Rhod 2-AM and 5 μM NP-EGTA-AM in a CO₂ incubator. Subsequently, the culture medium was gently rinsed with BSS. hRPE-YC cells were placed on an inverted confocal laser scanning microscope (FV1000, Olympus, Tokyo, Japan). Rhod 2 fluorescence images (598 nm) were acquired with a 543-nm HeNe laser and a 60 \times oil-immersion objective lens (UPLSAPO 60 \times /1.35, Olympus) and digital imaging software (FV10-ASW, Olympus). Time-lapse images were acquired over a 1-min period at 1-s intervals. For photolytic Ca²⁺ elevation, the target cell region was irradiated with 405-nm diode laser stimulation for 1 s using a Tornado-ScanTM system installed on the FV10-ASW. To analyse the effects of circadian time on the mitochondrial Ca²⁺ elevation, cells were pretreated with Dex as described above for *Bmal1-luc* counting prior to the imaging experiments.

Calcium imaging of rat SCN neurons in acute brain slices

To monitor mitochondrial Ca^{2+} in rat SCN neurons, acute hypothalamic slices containing the SCN (200–220- μm thickness) were prepared from Sprague–Dawley rats at postnatal day (PD) 9–13. The brains were removed under deep pentobarbital anaesthesia, and brain slices were cut in ice-cold high- Mg^{2+} artificial cerebrospinal fluid (ACSF) containing (mM) 138.6 NaCl, 3.35 KCl, 21 NaHCO_3 , 0.6 NaH_2PO_4 , 9.9 glucose, 0.5 CaCl_2 and 4 MgCl_2 using a vibrating blade tissue slicer. The SCN slices were incubated at room temperature for at least 30 min in regular ACSF (pH 7.4) containing (mM) 2.5 CaCl_2 and 1.0 MgCl_2 bubbled with 95% $\text{O}_2/5\%$ CO_2 . The SCN slices were then placed in a 0.40 μm culture insert and incubated at 30–32°C for 70–80 min in ACSF containing 10 μM NP-EGTA-AM, 5 μM Rhod 2-AM and 0.005% Cremophor EL, and bubbled with 95% $\text{O}_2/5\%$ CO_2 . Following rinsing of Rhod 2-AM with regular ACSF, the SCN slices were incubated with ACSF supplemented with 0.5 μM TTX and 2 μM nimodipine bubbled with 95% $\text{O}_2/5\%$ CO_2 at 30–32°C for 60 min, and then placed on a heating stage set at 33°C on an upright confocal laser scanning microscope (A1R MP plus). Rhod 2 fluorescence images (595 nm) were acquired with a 561-nm diode laser and a 25 \times water-immersion objective lens (Apo LWD 25 \times 1.10w DIC N2) and digital imaging software (NIS-Elements AR4.10). Time-lapse images were acquired as described above for hRPE cells.

Organotypic SCN cultures

The basic protocol for organotypic SCN cultures has been described previously (Ikeda et al., 2003). In this experiment, SCN slice cultures were prepared from PD3–5 Sprague–Dawley rats. The animals were deeply anesthetized with pentobarbital, and the brain was quickly removed and dropped into ice-cold high- Mg^{2+} ACSF bubbled with 95% $\text{O}_2/5\%$ CO_2 . Coronal hypothalamic slices (300- μm thickness) containing the SCN were cut using a vibrating blade tissue slicer and placed in 0.40- μm culture inserts. The inserts were placed in standard 6-well plates and cultured with 1 mL of medium comprising 50% basal medium Eagle, 25% Earle's balanced salt solution and 25% heat-inactivated horse serum, supplemented with 1% (v/v) GlutaMAX, 5 mg/mL glucose and 20 $\mu\text{g}/\text{mL}$ kanamycin. The cultures were maintained in a CO_2 incubator at $36 \pm 0.5^\circ\text{C}$ and 5% CO_2 .

Co-transfection of YC3.6, *Bmal1-luc* and *Letm1* shRNA into cultured SCN neurons

Reporter genes and shRNA probes were co-transfected into SCN cells using a gene-gun system as described previously (Ikeda and Ikeda, 2014). In this experiment, cultured SCN slices were co-transfected with *Yellow Cameleon (yc) 3.6* gene linked to a neuron-specific enolase promoter (pNSE/YC3.6) (Ikeda and Ikeda, 2014), *Bmal1-luciferase (Bmal1-luc)* reporter gene (Bp/527-Luc) (Yu et al., 2002), shRNA against rat *Letm1* or scrambled shRNA in RFP-C-RS vector (Letm1 Rat shRNA Plasmid Kit #TF700692) using a Helios Gene Gun System. For biolistics, gold particles were coated with the YC3.6 and *Bmal1-luc* expression vectors together with a vector carrying the shRNA against *Letm1*, scrambled shRNA or without these shRNA. The two or three vectors were suspended in Tris-EDTA buffer containing spermidine and then coated onto gold particles (1 μm , 5 mg for 50 bullets) according to the manufacturer's instructions. The gene-gun bullet was made using a Tubing Prep Station and blasted onto 7- to 10-day-old cultures with helium pressure (190–195 psi) using a Helios Gene Gun System.

Long-term calcium imaging in cultured SCN neurons

Calcium imaging in cultured SCN neurons was performed as described previously (Ikeda et al., 2003; Ikeda and Ikeda, 2014). The YC and RFP fluorescence levels at 3 days after transfection were observed using an inverted fluorescence microscope (Eclipse TE2000-s). The SCN slice that exhibited successful gene transfection was transferred to 35-mm glass-bottom dishes (glass diameter: 27 mm) and cultured with an interface volume (220 μL) of culture medium. On day 4 after gene transfection, the slices were transferred to a custom-built recording system composed of an inverted fluorescence microscope (DM IRB; Leica), stage heater box, 445-nm LED light source, excitation filter (445 nm DF10; Omega Optical), dichroic mirror (455DRLP; Omega Optical) and a 10 \times objective lens (HCPL Apo 10 $\times/0.40$; Leica). Two emission bandpass filters (480AF30 and 535DF25; Omega Optical) were switched using a filter changer wheel (Lambda 10-3, Sutter Instrument). The system was installed in a gas-tight black box filled with 5% CO_2 . The interior of the stage box was set at 36°C with saturating humidity. Fluorescent image pairs were acquired through an EM-CCD camera (Cascade 1K; Photometrics) at a sampling rate of one image-pair per 10 min for detecting circadian cytosolic Ca^{2+} oscillations. The electromagnetic shutter (Lambda10-B, Sutter Instrument), filter changer wheel and image acquisition were controlled using MetaFluor ver 6.1 imaging software.

Bmal1-luc imaging in cultured SCN neurons

The organotypic SCN slice cultures exhibiting successful gene transfection were confirmed by RFP fluorescence before luciferase imaging. Culture medium was then switched to a medium supplemented with 500 μM beetle luciferin, 1 day prior to the recording. The SCN slices were transferred to glass-bottom dishes (glass diameter: 27 mm) containing 220 μL of luciferin-supplemented medium. The SCN cultures were then incubated in a temperature-controlled (36°C) custom-built chamber attached to an inverted microscope stage (IX71; Olympus). The entire system was installed in a gas-tight black box filled with 5% CO_2 . The bioluminescence images were viewed using a 10 \times objective lens (UPlan Apo 10 $\times/0.40$; Olympus) and collected with a 30-min exposure time on a cooled EM-CCD camera (iXon Ultra Andor; controlled at -70°C with coolant circulation and 50% EM gain) attached at the bottom port of the microscope (i.e., outside of the black box). Image acquisition was controlled using MetaMorph imaging software. Z-plane focus was adjusted using a three-dimensional piezo motor-driven manipulator (Luigs & Neumann, Ratingen, Germany) attached on the

microscope stage at 45–49-h intervals by monitoring the RFP fluorescence image at the time of medium exchange. Although this system enables intermittent recordings of YC3.6 and *Bmal1-luc* from the same slice, we separately analysed Ca^{2+} and *Bmal1-luc* in different experiments because we observed luciferin fluorescence by 445-nm excitation in YC3.6 recordings.

Mitochondrial membrane potential assay

Mitochondrial membrane potentials in hRPE cells were measured using the fluorescent probe JC-1. Cells were seeded onto 35-mm plastic dishes in a CO_2 incubator. Cells were cultured to 60–70% confluence and then loaded for 60 min with 0.1 μM JC-1 dye in a CO_2 incubator. As a positive control, cells were treated with 50 μM FCCP for 60 min before staining. Subsequently, the culture medium containing JC-1 was gently rinsed from the dishes using BSS. Fluorescence images (535 nm and 590 nm) were acquired using an inverted microscope (Eclipse TE2000-s, Nikon) with a 20 \times objective lens (Plan Fluor ELWD 20 \times /0.45) and a xenon lamp (75 W). The red/green fluorescent intensity ratio was analysed using Image Pro Plus 7.0 software.

QUANTIFICATION AND STATISTICAL ANALYSIS

Data are presented as mean \pm standard error (SEM). Significant differences between two groups were analysed using two-tailed Student's *t*-test. Non-parametric analysis was conducted with the Mann–Whitney *U*-test. One-way analysis of variance (ANOVA) followed by Tukey's post hoc test or Kruskal–Wallis test were used for statistical comparisons across multiple means of a single factor. Additionally, two-way ANOVA was used to compare multiple means defined by two categorical factors. A four-parameter Hill function was used to estimate the calibration curve. A 95% confidence level was considered to indicate statistical significance. Statistical analyses were performed using the BellCurve add-in software for Microsoft Excel software. Cytosolic pH oscillations were analysed using a sinusoidal regression curve fitted with 95% confidence levels using SigmaPlot ver 7.0 software. Additionally, the pH-response curve for action potential firing frequencies was fitted by a four-parameter Hill function using SigmaPlot. Because the sampling interval for immunostaining studies was limited (6 points/24 h), sine curve fittings for PER/TIM expression rhythms were examined using CircWave version 1.4 software.